15. Kato T, Hirano A, Weinberg MN, Jacobs AK. Spinalcord lesion in progressive supranuclear palsy: somenew observations. *Acta Neuropathol* 1986; **71**: 11–14.
16. Kikuchi H, Doh-ura K, Kira J, Iwai T. Preferential neurodegeneration in the cervical spinal cord of progressive supranuclear palsy. *Acta Neuropathol* 1999; **97**: 577–584.
17. Iwasaki Y, Yoshida M, Hashizume Y, Hattori M, Aiba I, Sobue G. Widespread spinal cord involvement in progressive supranuclear palsy. *Neuropathology* 2007; **27**: 331–340.
18. Arai N, Oda M. **A** variety of glial pathological structures by the modified Gallyas-Braak method. *Neuropathology* 1996; **16**: 133–138.
19. Hauw JJ, Verny M, Delaere P, Cervera P, He Y, Duyckaerts C. Constant neurofibrillary changes in the neocortex in progressive supranuclear palsy. Basic differences with Alzheimer's disease and aging. *Neurosci Lett* 1990; **119**: 182–186.
20. Yamada T, McGeer PL, McGeer EG. Appearance of paired nucleated, tau-positive glia in patients with progressive supranuclear palsy brain tissue. *Neurosci Lett* 1992; **135**: 99–102.
21. Yamada T, Calne DB, Akiyama H, McGeer EG, McGeer PL. Further observations on tau-positive glia in the brains with progressive supranuclear palsy. *Acta Neuropathol* 1993; **85**: 308–315.
22. Nishimura T, Ikeda K, Akiyama H *et al.* Immunohistochemical investigation of tau-positive structures in the cerebral cortex of patients with progressive supranuclear palsy. *Neurosci Lett* 1995; **201**: 123–126.
23. Nishimura M, Namba Y, Ikeda K, Oda M. Glial fibrillary tangles with straight tubules in the brains of patients with progressive supranuclear palsy. *Neurosci Lett* 1992; **143**: 35–38.
24. Arima K. Ultrastructural characteristics of tau filaments in tauopathies: immuno-electron microscopic demonstration of tau filaments in tauopathies. *Neuropathology* 2006; **26**: 475–483.
25. Iwasaki Y, Yoshida M, Hattori M *et al.* Distribution of tuft-shaped astrocytes in the cerebral cortex in progressive supranuclear palsy. *Acta Neuropathol* 2004; **108**: 399–405.
26. Yoshida M. Cellular tau pathology and immunohistochemical study of tau isoforms in sporadic tauopathies. *Neuropathology* 2006; **26**: 457–470.
27. Boeve BF, Maraganore DM, Parisi JE *et al.* Pathologic heterogeneity in clinically diagnosed corticobasal degeneration. *Neurology* 1999; **53**: 795–800.
28. Togo T, Dickson DW. Tau accumulation in astrocytes in progressive supranuclear palsy is a degenerative rather than a reactive process. *Acta Neuropathol* 2002; **104**: 398–402.
29. Ahmed Z, Bigio H, Budka H *et al.* Globular glial tauopathies (GGT): consensus recommendations. *Acta Neuropathol* 2013; **126**: 537–544.
30. Gibb WR, Luthert PJ, Marsden CD. Corticobasal degeneration. *Brain* 1989; **112**: 1171–1192.
31. Riley DE, Lang AE, Lewis A *et al.* Cortical-basal ganglionic degeneration. *Neurology* 1990; **40**: 1203–1212.
32. Josephs KA, Tang-Wai DF, Edland SD *et al.* Correlation between antemortem magnetic resonance imaging findings and pathologically confirmed corticobasal degeneration. *Arch Neurol* 2004; **61**: 1881–1884.
33. Mizuno T, Shiga K, Nakata Y *et al.* Discrepancy between clinical and pathological diagnoses of CBD and PSP. *J Neurol* 2005; **252**: 687–697.
34. Murray R, Neumann M, Forman MS *et al.* Cognitive and motor assessment in autopsy-proven corticobasal degeneration. *Neurology* 2007; **68**: 1274–1283.
35. Ling H, O'Sullivan SS, Holton JL *et al.* Does corticobasal degeneration exist ? A clinicopathological re-evaluation. *Brain* 2010; **133**: 2045–2057.
36. Armstrong MJ, Litvan I, Lang AE *et al.* Criteria for the diagnosis of corticobasal degeneration. *Neurology* 2013; **80**: 496–503.
37. Feany MB, Dickson DW. Widespread cytoskeletal pathology characterizes corticobasal degeneration. *Am J Pathol* 1995; **146**: 1388–1396.
38. Heines MA, Guyot-Sionnest P. Synthesis and characterization of strongly luminsecing ZnS-capped CdSe nanocrystals. *J Phys Chem* 1996; **100**: 468–471.
39. Giepmans BN, Deerinck TJ, Smarr BL, Jones YZ, Ellisman MH. Correlated light and electron microscopic imaging of multiple endogenous proteins using Quantum dots. *Nat Methods* 2005; **2**: 743–749.
40. Uematsu M, Adachi E, Nakamura A, Tsuchiya K, Uchihara T. Atomic identification of fluorescent Q-dots on tau-positive fibrils in 3D-reconstructed Pick bodies. *Am J Pathol* 2012; **180**: 1394–1397.
41. Hirano A. A guide to neuropathology. IGAKU-SHOIN Tokyo, 1981.
42. Hattori M, Hashizume Y, Yoshida M *et al.* Distribution of astrocytic plaques in the corticobasal degeneration brain and comparison with tuft-shaped astrocytes in the progressive supranuclear palsy brain. *Acta Neuropathol* 2003; **106**: 143–149.
43. Hattori M, Yoshida M, Ojika K, Yuasa H, Mitake S *et al.* An autopsy case of corticobasal degeneration without prominent cortical pathology – an imitator of progressive supranuclear palsy (in Japanese with English astract). *Rinsho Shinkeigaku* 2000; **40**: 372–377.

44. Katsuse O, Iseki E, Arai T *et al.* 4-repeat tauopathy sharing pathological and biochemical features of corticobasal degeneration and progressive supranuclear palsy. *Acta Neuropathol* 2003; **106**: 251–260.
45. Tan CF, Piao YS, Kakita A *et al.* Frontotemporal dementia with co-occurrence of astrocytic plaques and tufted astrocytes, and severe degeneration of the cerebral white matter: a variant of corticobasal degeneration? *Acta Neuropathol* 2005; **109**: 329–338.
46. Tuite PJ, Clark HB, Bergeron C *et al.* Clinical and pathologic evidence of corticobasal degeneration and progressive supranuclear palsy in familial tauopathy. *Arch Neurol* 2005; **62**: 1453–1457.
47. Uchihara T, Mitani K, Mori H, Kondo H, Yamada M, Ikeda K. Abnormal cytoskeletal pathology peculiar to corticobasal degeneration is different from that of Alzheimer's disease or progressive supranuclear palsy. *Acta Neuropathol* 1994; **88**: 379–383.
48. Ikeda K. Basic pathology of corticobasal degeneration. *Neuropathology* 1997; **17**: 127–133.
49. Arai T, Ikeda K, Akiyama H *et al.* Identification of amino-terminally cleaved tau fragments that distinguish progressive supranuclear palsy from corticobasal degeneration. *Ann Neurol* 2004; **55**: 72–79.
50. Shibuya K, Yagishita S, Nakamura A, Uchihara T. Perivascular orientation of astrocytic plaques and tuft-shaped astrocytes. *Brain Res* 2011; **1404**: 50–54.

Tatsumi et al. Acta Neuropathologica Communications 2014, 2:161
http://www.actaneurocomms.org/content/2/1/161

ACTA NEUROPATHOLOGICA COMMUNICATIONS

RESEARCH Open Access

Ultrastructural differences in pretangles between Alzheimer disease and corticobasal degeneration revealed by comparative light and electron microscopy

Shinsui Tatsumi[1,2,3], Toshiki Uchihara[2*], Ikuko Aiba[4], Yasushi Iwasaki[1], Maya Mimuro[1], Ryosuke Takahashi[3] and Mari Yoshida[1]

Abstract

Pretangles are defined under the light microscope as diffuse and granular tau immunoreactivity in neurons in tissue from patients with Alzheimer disease (AD) or corticobasal degeneration (CBD) and are considered to be a premature stage before neurofibrillary tangle formation. However, the ultrastructure of pretangles remains to be described. To clarify the similarities and differences between pretangles from patients with AD and CBD (AD-pretangles and CBD-pretangles, respectively), we examined cortical pretangles in tissue from patients with each of diseases. For direct light and electron microscopic (LM/EM) correlation of the pretangles, we used quantum dot nanocrystals (QDs) with dual fluorescent and electron-dense properties. We first identified tau-labeled pretangles on fluorescence LM and subsequently examined the same neurons on EM. Energy dispersive X-ray spectrometry (EDX) color mapping identified selenium (Se) and cadmium (Cd) as elementary components of QDs and highlighted each QD particle clearly against gray-scale EM images. With these methods, we were successful for the first time in demonstrating accurately that LM-defined pretangles are tau-positive straight filaments sparsely distributed throughout neuronal cytoplasm and neurites in both AD and CBD at the EM level. Notably, AD-pretangles showed a strong tendency to form fibrillary tangles even at an early stage, whereas pretangles or Pick-like inclusions in tissue from patients with CBD did not even at an advanced stage. In conclusion, AD-pretangles and CBD-pretangles showed essential differences at the EM level.

Introduction

Changes that occur in relevant molecules before they become organized into disease-specific inclusions in human brains are attracting increasing attention [1]. The pretangle is an example of such an early change; it was originally defined under light microscopy (LM) as diffuse and granular tau immunoreactivity in the cytoplasm and neurites of otherwise intact neurons in brains from patients with Alzheimer disease (AD) [2-4]. Mature neurofibrillary tangles (NFTs), which are hallmarks of AD, are readily identified as bundles of paired helical filaments (PHFs) under electron microscopy (EM) [5]. However, it is difficult to identify pretangles under EM because their faint tau immunoreactivity suggests that their ultrastructure is less distinct. Although putative ultrastructures of pretangles in AD have been reported, it is not yet clarified whether they really represent neurons containing diffuse and granular tau immmunoreactivity as defined under LM [2]. Similar granular tau immunoreactivity has also been observed in corticobasal degeneration (CBD), a four-repeat tauopathy that causes degeneration of the cerebral cortex, basal ganglia, and substantia nigra. Because they appear similar to AD-pretangles under LM, this granular tau immunoreactivity is also known as pretangles. Pretangles are considered one of the most important neuronal cytopathologies in CBD [6,7] but are also found in argyrophilic grain disease or progressive supranuclear palsy [8].

* Correspondence: uchihara-ts@igakuken.or.jp
[2]Laboratory of Structural Neuropathology, Tokyo Metropolitan Institute of Medical Science, 2-1-6 Kamikitazawa, Setagaya, Tokyo 156-8506, Japan
Full list of author information is available at the end of the article

The aim of this study was to visualize the ultrastructures of LM-defined AD- and CBD-pretangles and thereby to identify possible differences between them. For this purpose, it is necessary to directly compare LM and EM images of the same pretangle, an approach that is now named "correlative light and electron microscopy (CLEM)". Although CLEM protocols have been developing [9-17], they usually allow LM/EM comparisons for only small fields (the size of the EM preparation). This limitation makes it practically impossible to capture pretangles for immunoEM study because pretangles are not sufficiently frequent to be included by chance in such tiny preparations. Therefore, it is necessary to excise tissue containing a pretangle from the LM sample before it can be prepared for EM.

Quantum dots (QDs) are fluorescent, electron-dense semiconductor nanocrystals of uniform size with a core of cadmium selenide [18]. On EM examination, QDs also display a characteristic peripheral halo [19]. These dual optical properties allow QDs to be identified under both LM and EM and therefore permits labeled LM structures to be compared directly with their ultrastructures [16]. Using QDs, we recently established three dimension (3D) - oriented immunoelectron microscopy [19,20]. In this method, a thick floating section from the formalin-fixed human brain is incubated with the primary and QD-conjugated secondary antibodies. After a target neuron is examined with fluorescent LM (confocal microscopy), landmarks are punched out around the neuron using laser microdissection. Then, this floating section is processed for EM preparation. The advantage of this stepwise LM-EM approach is that the neuron of interest can be observed closely on confocal microscopy prior to the EM examination, and its EM findings can be supplemented with confocal images because the same reporter (i.e., QDs) can been seen under both LM and EM immunostaining.

Although QDs provide a powerful bridge between LM and EM, their electron density is lower and their contour is less distinct than those of gold particles, leading to doubts about QD use as an immunolabeling material for EM. We previously overcame this problem using energy dispersive X-ray (EDX) spectrometry, which demonstrated parallel peaks corresponding to selenium (Se) and cadmium (Cd) on the pixels for definitive confirmation of QDs on EM preparations [19]. Because it is possible to obtain EDX spectrum for each pixel, we extended this pixel-based EDX analysis to plot the entire EM field pixel by pixel in this study. Operational display of pixels containing Cd peak or those containing Se peak highlighted QD particles based on their elemental composition with different colors. When it was overlaid onto the conventional gray-scale EM image, this EDX color mapping clearly distinguished QDs from background structures such as ribosomes.

With these methods, it is possible to examine the ultrastructural details of AD- and CBD-pretangles and to elucidate their similarities and differences at the EM level [2-4,6]. Using this LM/EM correlation with novel mapping method, we obtained an EM image of the early stage of neuronal tau deposition in AD-pretangles and found essential differences between AD- and CBD-pretangles at the EM level. This is the first successful demonstration of their ultrastructural differences.

Materials and methods

Alzheimer disease and corticobasal degeneration cases

To investigate the ultrastructure of pretangles, we compared them in different diseases with different severities (Table 1). We used samples from one case of AD, a case of normal aging, and two typical cases of CBD. The diagnoses of AD and CBD were based on the current diagnostic criteria [6,21]. Identification of pretangles was based on LM findings as "cytoplasmic diffuse and granular tau immunoreactivity without apparent fibrillary structures". In the normal aging samples, pretangles and Alzheimer-type NFTs were localized to the hippocampus and the parahippocampal cortex. In the CBD samples, we examined

Table 1 Demographic features of cases with AD, normal aging, and CBD

	Pathological diagnosis	Age of death (y)/sex	Brain weight (g)	Duration (y)	Braak NFT stage	Clinical symptoms	Type of tau-positive inclusions investigated
Case 1	Normal aging	73/F	1,260	na	I	No history of dementia or motor symptoms	Pretangles, NFTs
Case 2	AD	58/F	850	14	VI	Severe dementia, disorientation	Pretangles, NFTs
Case 3	CBD	60/M	1,145	7	I	Supranuclear gaze palsy, frequent fall, parkinsonism, frontal signs	Pretangles, Pick-like inclusions*
Case 4	CBD	70/F	770	11	III	Frontotemporal dementia, parkinsonism	Pretangles, Pick-like inclusions, ballooned neurons

*Pick-like inclusions denoting densely packed round inclusions usually observed in the small-sized cortical neurons in corticobasal degeneration; AD, Alzheimer disease; CBD, corticobasal degeneration; NFT, neurofibrillary tangle.

pretangles and densely packed round inclusions (Pick-like inclusions) [6] in the frontal lobe.

Pre-embedding tau/QD labeling for LM/EM observation

Formalin-fixed brains were rinsed in phosphate-buffered saline (PBS) and cryoprotected in 20% sucrose/PBS overnight. The tissue was frozen in optimal cutting temperature (OCT) compound and cut into 25-μm-thick floating sections on a freezing microtome. The sections were immersed in 1% bovine serum albumin/PBS for 30 min and then incubated in anti-PHF tau antibody (AT8, mouse, monoclonal, 1:700; Thermo Fisher Scientific, Tokyo, Japan) for 24 hours at room temperature (RT). After washing in PBS for 30 min, sections were incubated in an anti-mouse secondary antibody conjugated to Q-dot 655 (QD 655) (goat, 1:100 to 1:800, diluted in PBS; Invitrogen, Carlsbad, CA) for 8 hours at RT. A QD 655 dilution at 1:400 (Additional file 1: Figure S1) for a CBD pretangle provided appropriate immunoEM labeling on tau-positive filaments, whereas its fluorescent signal was not intense enough to delineate subcellular details under confocal microscopy (Additional file 1: Figure S1). Therefore, the QD-labeled sections were subsequently incubated in an anti-mouse secondary antibody conjugated to Alexa 488 (goat, 1:200; Molecular Probe) for 3 hours at RT to allow more detailed LM observation. After incubation, sections were rinsed in PBS and then mounted in fluorescence-mounting medium (S3023; Dako, Glostrup, Denmark).

Confocal LM observation and EM preparation

Three-dimensional reconstruction images of the pretangles were obtained under fluorescence confocal microscopy (LSM 710; Carl Zeiss, Oberkochen, Germany) using a 63 × –oil immersion objective lens. Alexa 488 was excited using an argon laser (488 nm), and the detection bandwidth was set at 493 to 601 nm (expected peak at 520 nm). QD 655 was excited with a diode laser (405 nm), and the detection bandwidth was set at 605 to 690 nm (expected peak at 655 nm), which gave essentially the same image as obtained with Alexa 488 [19]. A Z-series scan (800 × 800 pixels, interval 0.40 μm, approximately 10-μm thick in total) was performed for 3D reconstruction. After obtaining 3D data sets with the confocal microscope, landmarks were punched out around the target neurons using the UV laser Micro dissection system PALM (P.A.L.M. Microlaser Technologies, Bernried, Germany) (Figure 1). The sections were then detached from the glass slide, fixed in 2% glutaraldehyde for 10 min, and postfixed in 1% osmium tetroxide for 30 min. Next, the sections were embedded in epon as follows: they were gently pressed between aclar films (Nissin EM catalog #4513, Tokyo, Japan) so that flat preparation on epon was possible and then hardened with heat (60°C). An aclar film on one side was detached from the hardened epon-embedded section. Then, the section was stuck to columnar epon that had been prepared in advance (Figure 1). The target-oriented trimming of the epon block was facilitated by the guidance of punched out landmarks around the target already identified and 3D-reconstructed on confocal microscopy. Ultrathin sections of the trimmed blocks were stained with uranyl acetate/lead citrate and examined with a JEM-1400 electron microscope (JEOL, Tokyo, Japan). After obtaining the most appropriate EM images, their exact LM counterpart was retrieved from the corresponding fluorescent 3D data set for direct comparison (Figure 1).

Energy dispersive X-ray (EDX) spectrometry and elemental mapping of QDs

The EM sections were also observed under a Hitachi HD-2700 scanning transmission electron microscope (STEM, Hitachi High Technologies Corporation, Tokyo, Japan). This STEM is equipped with a cold-field emission gun and detectors that consist of bright-field, high-angle annular dark-field (HAADF) and secondary electron (SE) detectors, which distinguish different elements (Cd and Se in this experiment) based on their energy spectra on a pixel basis. This approach identifies the presence of Cd and Se in each STEM pixel. This pixel-based identification of Cd and Se is then extended to map the entire EM field to delineate the QD particles in relation to underlying ultrastructures. The STEM was operated at 200 kV and an EDX spot analysis was performed with an incident beam size of 0.2 nm and a current of 0.4 nA. The acquisition time for each pixel was 200 μsec. In the EDX mapping, the EDX analysis was performed in a 0.4 μm × 0.5 μm field, and the total acquisition time was 90 min. Pixels containing Se or Cd peaks were displayed on the EM field independently in different color channels.

Results

EDX analysis and EDX mapping of QDs

The shape of electron-dense QD 655, dribbled on the formvar membrane, was spherical to oblong on the STEM image (Additional file 2: Figure S2A). Pixel-based EDX elementary mapping highlighted the distribution of Se and Cd (Additional file 2: Figure S2B and D, respectively), which exactly corresponded to the ultrastructural shape of QDs (Additional file 2: Figure S2C). In a CBD-pretangle (case 3) examined using a QD 655-conjugated secondary antibody, tau filaments were labeled with numerous QDs of similar morphology (Figure 2A). The EDX spot analysis identified these QDs on the basis of energy peaks corresponding to Se and Cd. Elemental mapping with this EDX analysis further showed the distribution of QDs based on the presence of Se and Cd (Figure 2B). As mentioned, when the original STEM image was overlaid onto this

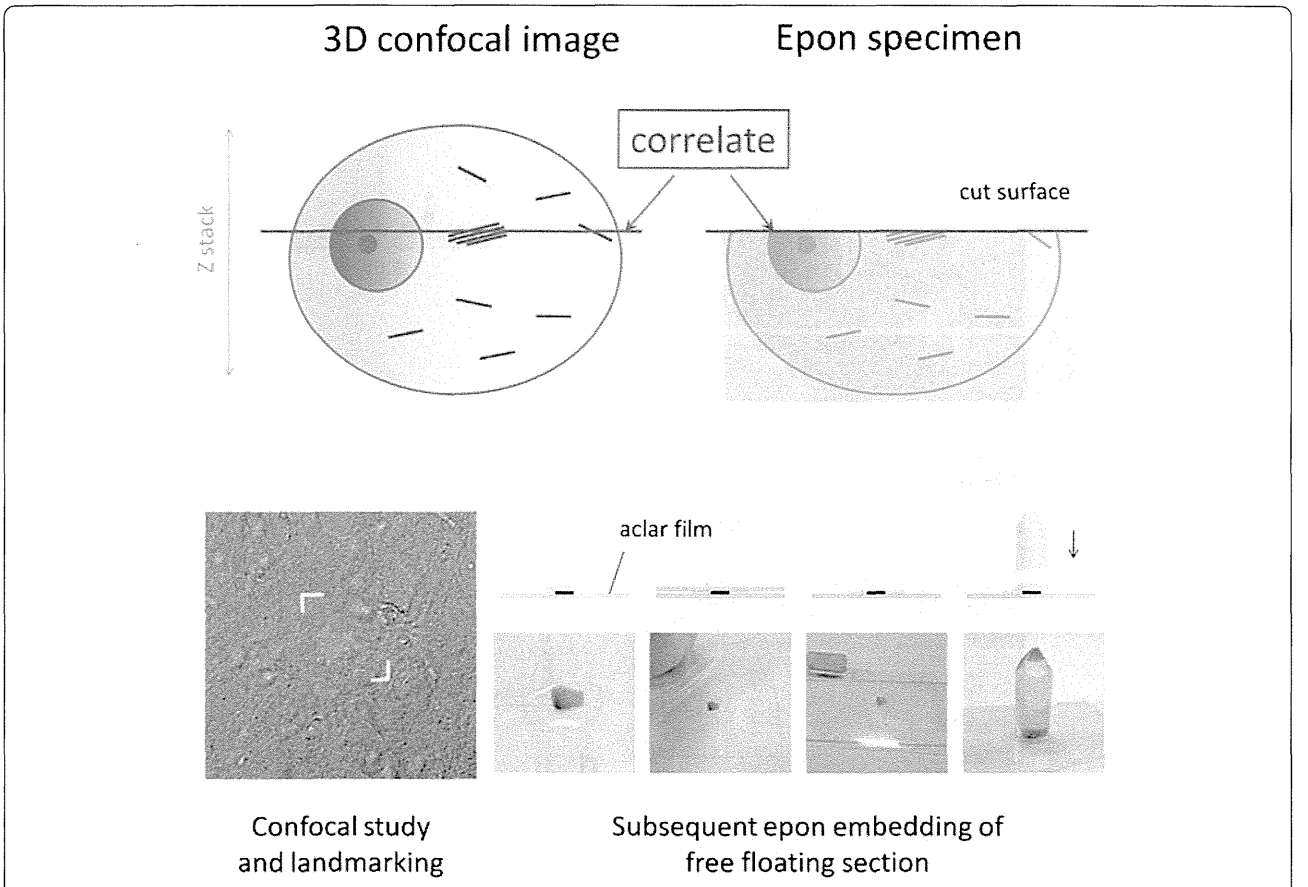

Figure 1 Outline of correlation of confocal and EM images. Three-dimensional (3D) reconstructed confocal data of the pretangles were obtained from a free-floating section. After landmarks were punched out around the target neuron using laser microdissection, sections were fixed and embedded in epon: the section was gently pressed between aclar films, hardened, then stuck to the columnar epon prepared in advance. The epon block was trimmed by the guidance of landmarks around the neuron, and ultrathin section of the block were examined with electron microscopy (EM). After obtaining the most appropriate EM images, their exact light microscopic counterparts were retrieved from the corresponding fluoresent 3D data set for direct comparison.

EDX mapping, the regional distributions of these analytical QD signals were identical to the ultrastructural shapes of QDs (Figure 2C). With this technique, the QDs could be readily differentiated from the grayscale background, even if the tau-filaments were intermingled with (similarly round) ribosomes (Figure 2C, arrow).

LM findings and corresponding ultrastructures of pretangles in AD and aging

Confocal examination of AD-pretangles revealed a mixture of granular tau immunoreactivity and small tangle formation (Figure 3A, stacked 3D image). When an EM section (C) and the corresponding LM counterpart on the same plane (B) were compared, the tangle-like aggregate (B, arrow; C, rectangle d) was found to be a small bundle of straight filaments tightly arranged in parallel (D), which is indistinguishable from mature NFTs in AD (Figure 3B-D). Such a precise comparison on the corresponding planes of LM and EM was not possible between 3D stacked image (A) and the EM section (C). In contrast, granular immunoreactivity on the LM plane (B), corresponded to straight filaments randomly and sparsely distributed throughout the cytoplasm (arrowheads, E), probably representing an earlier stage before bundle formation (Figure 3B, C, E). Occasional paired helical filaments (PHFs) were observed in AD-pretangles (Figure 3F). The distribution of these tau filaments was so sparse that they could be identified on EM only with dual guidance through subcellular orientation using a LM image and QD immunolabeling. Perinuclear staining was sometimes found in AD-pretangles on confocal images (G: stacked 3D image and corresponding plane on LM (H) and EM (I)). This corresponded to a low density of immunolabeled straight filaments attached to the nuclear membrane (Figure 3I, J, asterisk). The diameter of straight filaments ranged from 14 to 16 nm, and the period of filament constriction was 70 to 90 nm in AD and normal aging cases.

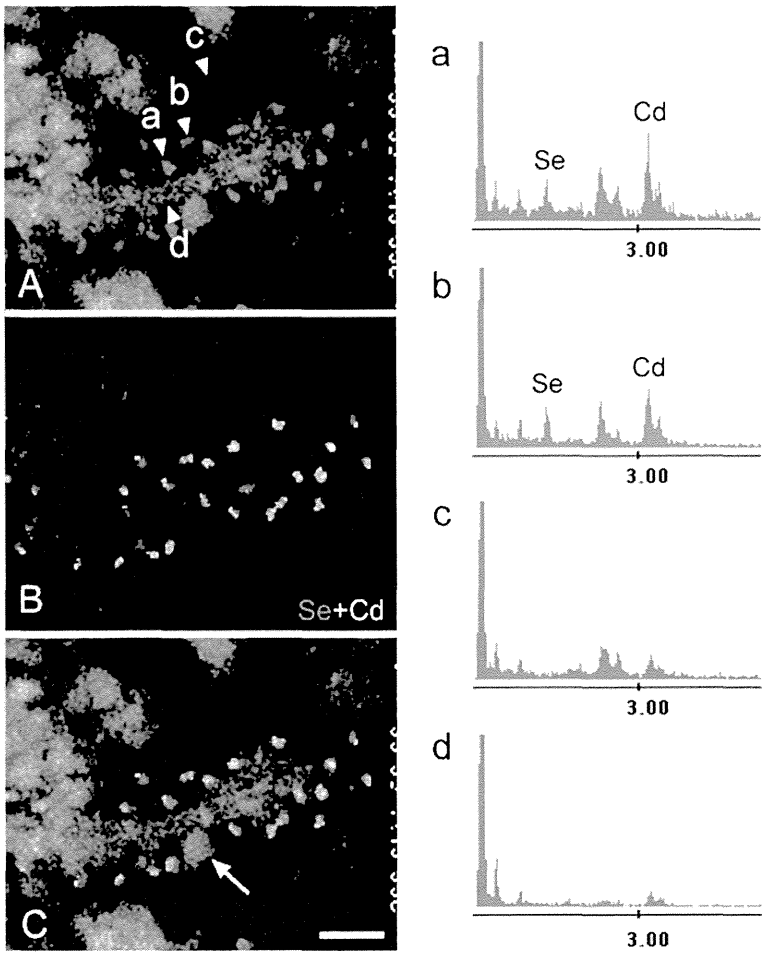

Figure 2 EDX mapping of QDs around tau-positive straight filaments in a case of CBD. EDX spot analysis of the section highlighted energy peaks corresponding to Se and Cd on QDs (Arrowheads **a** and **b** in panel **A** correspond to energy spectra **a** and **b**), but not on the background (arrowhead **c**) and the filament itself (arrowhead **d**). This pixel-based identification of Cd and Se is then extended to map the entire EM field to delineate the QD particles in relation to underlying ultrastructures. This approach produced Se (pink)- and Cd (yellow)-specific signals derived from QDs **(B)** as a map independent of underlying ultrastructures. The QDs were easily distinguished from a ribosome (arrow) (overlay, **C**). Scale bar = 50 nm.

LM findings and corresponding ultrastructures of CBD-pretangles

CBD-pretangles, which were often found in the superficial and deep layers of the cerebral cortex, were characterized by diffuse and reticular (rather than granular) immunoreactivity in the neuronal cytoplasm with few solid aggregates (Figure 4A). The density of the reticular structures varied from cell to cell or from case to case. 3D observations using confocal microscopy showed that the reticular structures extended into the distal portions of dendrites (Figure 4A). Perinuclear tau immunoreactivity, as seen in AD-pretangles, was not observed in CBD-pretangles. Correlation of the LM and EM images demonstrated that reticular structures seen by confocal microscopy corresponded to straight filaments, which were diffusely and randomly distributed throughout the cytoplasm and did not displace cellular organellae (Figure 4A-C, E). In dendrites, a few straight filaments were assembled in a roughly parallel fashion. Their arrangement was less tight than in NFTs in AD (Figure 4D). In tissue from the more severe case of CBD (case 4), reticular structures were denser on both confocal microscopy and EM images than in case 3 (Figure 5A- E). Interestingly, straight filaments were thicker in diameter in case 4 (15–20 nm) than in case 3 (14 to 15 nm). Straight filaments also appeared longer in case 4. In this study, PHFs were not observed in CBD-pretangles in either case.

Ultrastructure of Pick-like inclusions in small neurons in two CBD cases

Densely packed round inclusions (Pick-like inclusions) were found mainly in the small neurons in the superficial layer of the cerebral cortex of CBD cases; their tau

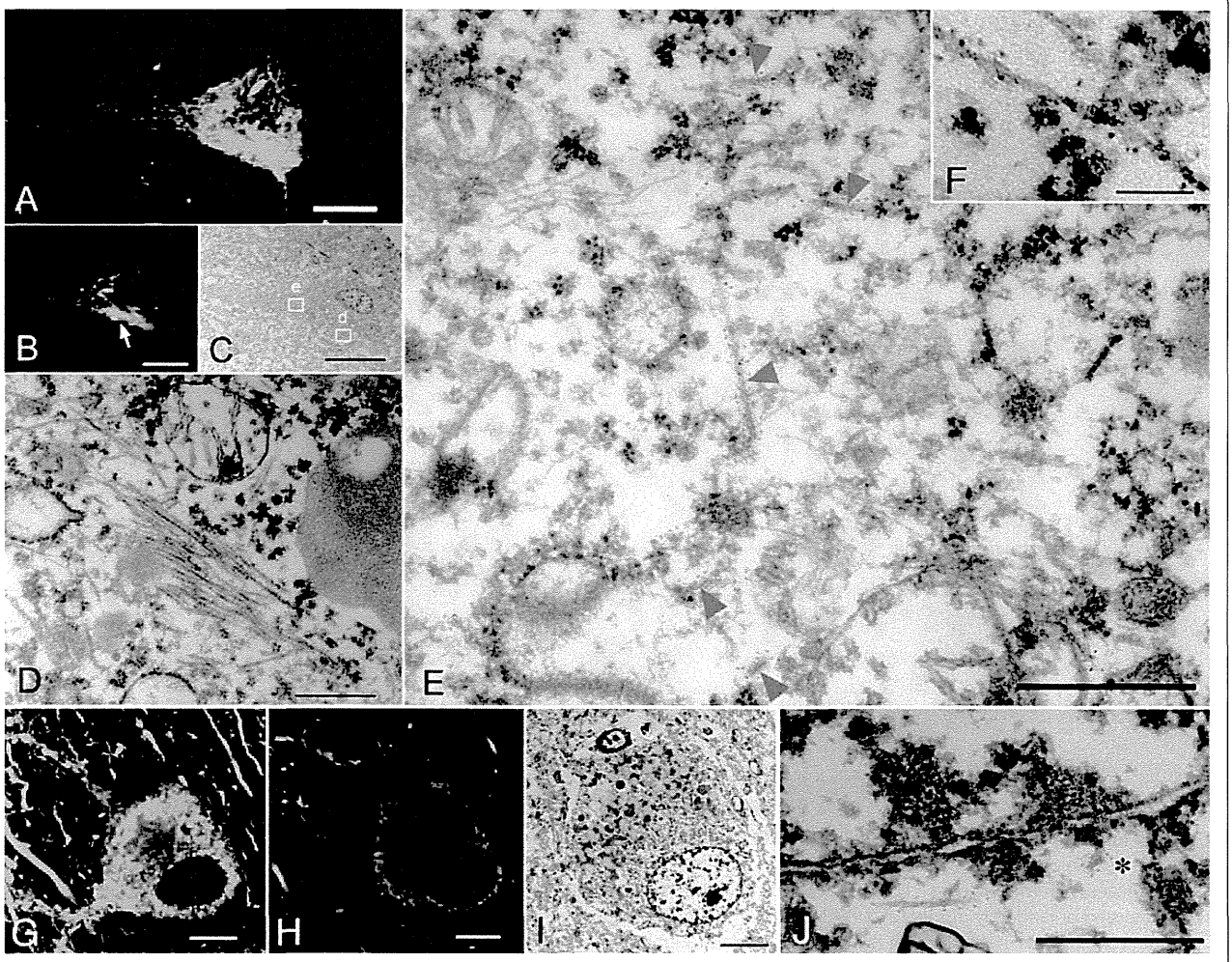

Figure 3 Correlation of immunolabeled LM and EM images of Alzheimer disease (AD)-type pretangles. A mixture of granular tau immunoreactivity and tangle-like aggregates in a pretangle neuron from a normal aging brain (case 1) (**A**, stacked 3D image). This neuron was labeled with anti-tau antibody(AT8) visualized with QD 655, also labeled with Alexa 488 for clearer confocal images. When an EM section **(C)** and the corresponding LM counterpart on the same plane **(B)** were compared, the tangle-like aggregate (**B**, arrow; **C**, rectangle d) was found to be a small bundle of straight and paired helical filaments tightly arranged in parallel **(D)**. Granular immunoreactivity on LM (**C**, rectangle e) corresponded to 15-nm straight filaments widely and randomly distributed throughout the cytoplasm on EM **(E)**. Paired helical filaments were occasionally seen in pretangle neurons of AD **(F)**. Another pretangle neuron with perinuclear accentuation of tau immunoreactivity (**G**, stacked 3D image; case 2). EM image **(I)** and the corresponding LM counterpart on the same plane **(H)** were compared, QD-decorated straight filaments were seen around the nucleus (N) and some of them were attached to the nuclear membrane at the tip (asterisk, **J**). Scale bars in **A-C, G-I** = 5μm; **D, E, J** = 500 nm; **F** = 100 nm.

immunoreactivity was more compact and denser than that of CBD-pretangles. On confocal observation, we found that these inclusions often contained small cavities (Figure 6A-B). The correlation of LM and EM images revealed bundles of tau filaments around the cavities (Figure 6B-D). Tau-positive filaments were composed of straight filaments and PHFs with a periodicity of approximately 130 nm (Figure 6D-E). These filaments were loosely assembled and usually intermingled with cellular organellae, especially ribosomes (Figure 6D, arrow). Strictly speaking, the straight filaments were not oriented parallel to each other. The diameters of straight filaments in these inclusions ranged from 13 to 15 nm in case 3 and 15 to 16 nm in case 4. Similarities and differences among AD-pretangles, NFTs in AD, CBD-pretangles, and Pick-like inclusions in CBD are listed in Table 2.

Among hundreds of AT8-positive neurons on confocal, 3–4 pretangles were selected in each AD and CBD case, which were 3D-reconstructed and prepared for EM observation. In addition, 3–4 Pick-like inclusions were selected in each CBD case and were processed similarly.

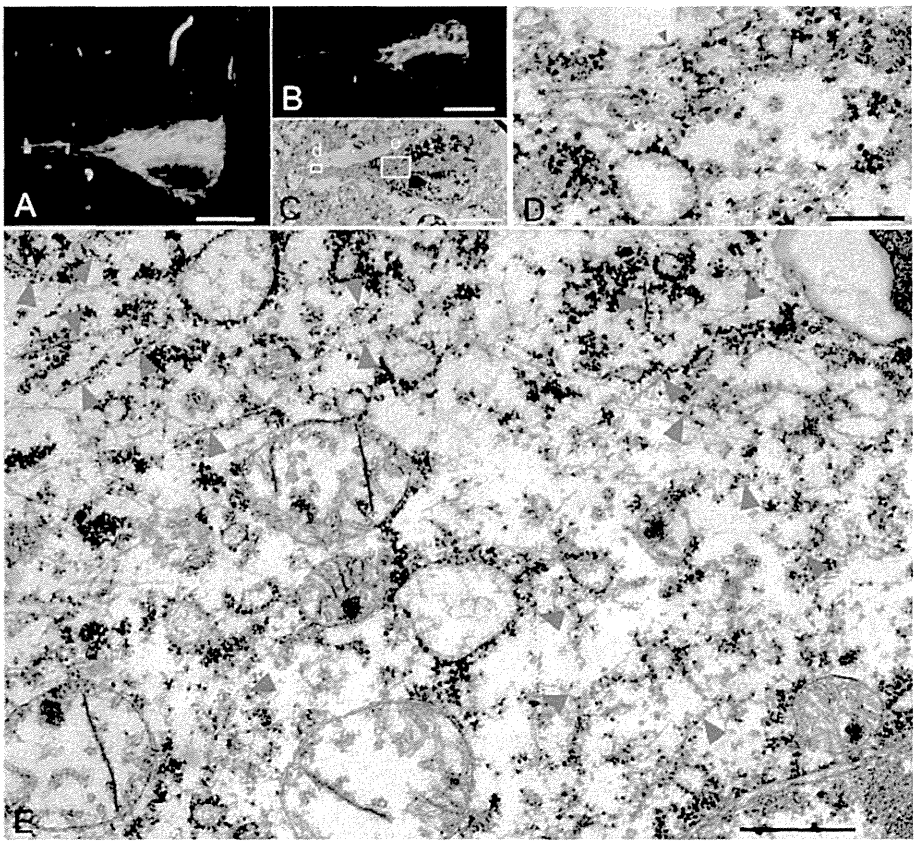

Figure 4 Correlation of immunolabeled LM and EM images of CBD-pretangles. Reticular tau immunoreactivity in the cytoplasm in a pretangle neuron of CBD (case 3) labeled with anti-tau antibody (AT8) visualized with QD 655, also labeled with Alexa 488 for more precise confocal images **(A)**. When compared between LM **(B)** and its exact EM counterpart, reticular tau immunoreactivity in the cytoplasm (**C**, rectangle e) was composed of randomly distributed straight filaments (**E**, arrowheads). Tau immunoreactivity in the dendrite (**C**, rectangle d) on LM corresponded to a few 15-nm straight filaments assembled roughly in parallel. Their arrangement was less tight than that in NFTs in AD. Scale bars in **A-C** = 10 μm; **D** = 250 nm; **E** = 500 nm.

Discussion

The name 'pretangle' was originally used to describe the premature stage of NFT formation in AD [2-4]. However, in CBD, similar structures (also called 'pretangles') are more prevalent than NFTs in the cerebral cortex [6]. It has been unclear whether the pretangles of CBD represent a premature stage before NFT formation and whether they are different from AD-pretangles. Because pretangles are defined only by LM findings [2-4], it would be helpful to compare the corresponding pretangle ultrastructures between the two diseases. However, CBD pretangles in the cortex have not previously been described at the EM level [22-28]. To address this issue, we used a method of correlative light and electron microscopy with QD immunolabeling [19]. This procedure allowed us to observe not only the features of filamentous structures of inclusions but also their intracellular distribution and relationship with cellular organellae.

Using correlated LM and EM images, we observed a distinctive EM feature of AD-pretangles: specifically, a strong tendency to form bundles as a precursor to NFTs. Even in the earliest stages of tau accumulation, small pieces of NFTs could already been seen on the background of diffuse and granular tau staining on LM (Figure 3A) [3,29]. Correlation of the LM and EM images revealed that the granular cytoplasmic staining on LM represented straight filaments (sparsely distributed in the neuronal cytoplasm), and the small tangles represented small bundles of parallel filaments (Figure 3D). Very similar EM findings were reported by Bancher [2], although it remains unclear whether their EM findings really represented LM-defined pretangles or not. Because our method of 3D-oriented immunoEM not only identify pretangles on LM, it is quite sure that our immuno EM findings represent LM-identified pretangles. Moreover, it is further possible to correlates the EM plane (Figure 3C) and its exact counterpart of the corresponding LM plane (Figure 3B), even a small aggregates (Figure 3B arrow) not identifiable on 3D stack image (Figure 3A) can be examined with EM (Figure 3C) for comparison with LM at the extreme

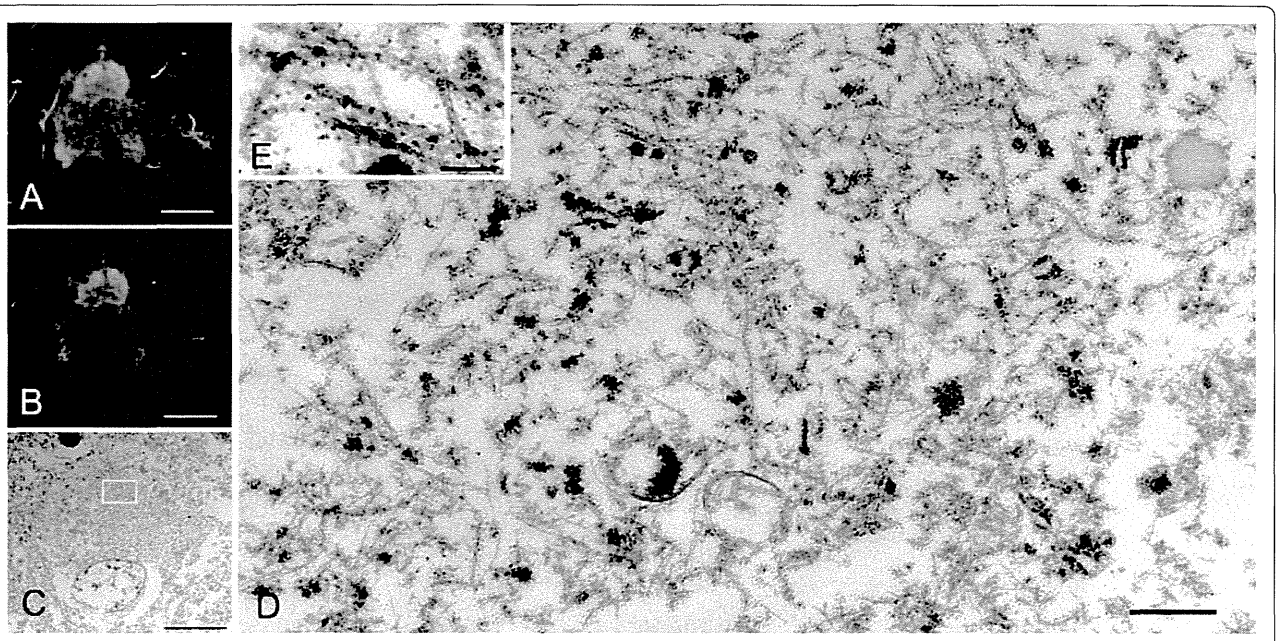

Figure 5 Correlation of immunolabeled LM and EM images of pretangles in a severe case of CBD. In a pretangle neuron from a severe case of CBD (case 4), reticular tau immunoreactivity was denser on 3D reconstruction **(A)**. When focusing on the denser area of round inclusion **(B, C)**, the corresponding EM section contained abundant tau-positive straight filaments that did not form a parallel arrangement **(D)**. These straight filaments were thicker with a diameter of 15–20 nm **(E)**. Scale bars in **A-C** = 10 μm; **D** = 500 nm; **E** = 100 nm.

accuracy. Another feature of AD-pretangles was perinuclear accumulation of tau. Correlation with its EM counterpart showed that a small number of tau-positive 15-nm straight filaments were present around the nuclear membranes of AD-pretangles (Figure 3G-J). It has been reported that PHF or tau-like immunoreactivity may be present in close proximity to the nuclear membrane of mature NFTs in AD [29-32], and this report is the first demonstration of tau-immunolabeled filaments around the nuclear membrane of AD-pretangles. Although intranuclear processes such as aberrant cell cycling may be related to the pathogenesis of AD [33,34], it is unclear how these processes are related to the perinuclear or cytoplasmic deposition of tau.

A similar approach to CBD-pretangles of the cerebral cortex revealed several findings that differed from the features of AD-pretangles and NFTs: (i) random and diffuse distribution of 14–20 nm straight filaments and (ii) paucity of PHFs and fibrillary bundle formation. These ultrastructural architectures may explain the reticular or diffuse tau immmunoreactivity of CBD-pretangles seen on LM (Figures 4 and 5). In dendrites, a small number of straight filaments were observed lying parallel to the dendritic shaft (Figure 4D), similar to the previous reports of dendritic lesions in CBD [8,22]. Even in CBD-pretangles with abundant tau filaments, this random and diffuse distribution of straight filaments was maintained with little NFT formation (Figure 5D). Indeed, this architecture was maintained even in Pick-like inclusions, where tau filaments were randomly assembled and were composed mainly of straight filaments and, to a lesser extent, PHFs with a periodicity of 130–180 nm (Figure 6D-E). Thus, so-called CBD-pretangles are a random accumulation of tau-positive straight filaments, rarely evolving into so-called NFTs even when the filament density is increased. These findings, especially regarding the filamentous structures themselves, were similar to previous findings in CBD (15–20 nm straight filaments or PHFs with a periodicity of 120–180 nm), which were observed in Pick-like inclusions [22-24,27], ballooned neurons [24,28], neuronal inclusions in the brainstem [22,26,28], or an *in vivo* study using CBD brains [25]. However, this study is the first to clarify the EM structures of cortical pretangles in CBD by accurately correlating them with LM images. Authentic Pick bodies in Pick body disease were more solid than pretangles on LM, where abundant tau-positive fibrils, 15 nm in diameter, were randomly arranged without forming PHF [19].

In this study, we greatly enhanced the reliability of pre-embedding immunoEM using QDs. Although QDs are considered suitable for CLEM, their reliability as a reporter for ultrastructural immunolabeling has been debated. The penetration of QD labeling is reported to be limited to several micronmeters from the sample surface [15]. However, we were successful in immunolabeling 25-μm-thick free-floating sections by increasing the incubation time with QD-conjugated secondary antibodies to 8 hr at room temperature. This procedure enabled us

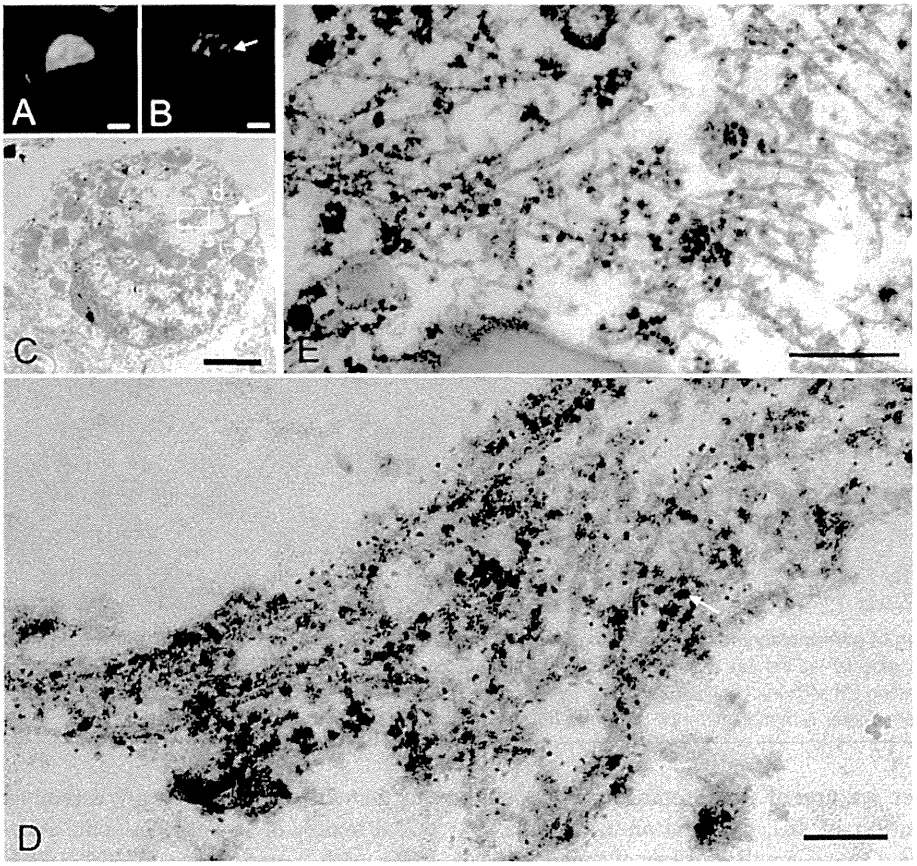

Figure 6 Correlation of immunolabeled LM and EM images of Pick-like inclusions in two CBD cases. A densely packed round inclusion (Pick-like inclusion) from a CBD case (case 3) labeled with anti-PHF antibody (AT8) visualized with QD 655, also labeled with Alexa 488 for more precise confocal images **(A)**. Correlated LM and EM images **(B, C)** showed that tau immunoreactivity around the cavity on LM corresponded to bundles of tau filaments that were not arranged as parallely as in AD (**C**, rectangle d; **D**). Note that these filaments were intermingled with ribosomes (**D**, arrow). **(E)** The ultrastructure of Pick-like inclusions in another case of CBD (case 4) also revealed randomly assembled tau filaments with occasional formation of paired helical filaments (a periodicity of 130 nm, arrow). Scale bars in **A** to **C** = 3 μm; **D** = 50 nm; **E** = 100 nm. **A** to **D**, case 3; **E**, case 4.

Table 2 Similarities and differences between AD-pretangle and CBD-pretangle

		AD		CBD	
		Pretanle	**NFT**	**Pretangle**	**Pick like inclusion**
LM findings (confocal images)	Morphology	Granular	Fibrillary	Reticular	Round, frequent vacuoles
	Perinuclear accentuation	Occiasional	Occasional	None	None
	Size of neurons involved	Small- to large- sized	Small- to large- sized	Medium- to large-sized	Small-sized
EM findings	Density of tau filaments	Very sparse*1	Very dense*2	Sparse	Dense
	Arrangement of tau filaments	Irregular/regular (focal NFT formation*3)	Regular (NFT formation)	Irregular	Irregular
	Diameter of straight filaments	About 15 nm	About 15 nm	14-20 nm	About 15 nm
	PHF (a periodicity)	Occasional (about 80 nm)	Frequent (about 80 nm)	None	Occasional (130–180 nm)

IHC, immunohistochemistry; LM, light microscopy; EM, electron microscopy; PHF, paired helical filaments; *1, Density of straight tau filament is more sparse in AD-pretangles than in CBD-pretangles; *2, Density of tau filaments is more dense in AD-NFT than in Pick-like inclusions of CBD; *3, NFT, neurofibrillary tangle signifying a regularly and tightly arranged bundle of straight or paired helical filaments.

to label the entire thickness of floating sections with QDs so that each tau filament was sufficiently labeled (Figures 3 and 4). Consequently, confocal images and immunoEM images could be tightly correlated.

Other disadvantages of QDs are that they have a lower electron density and less distinct contours than colloidal gold for immunolabeling. We previously used EDX spot analysis with STEM to demonstrate the presence of Se and Cd on a pixel basis [19]. This EDX spot analysis, now extended to map the entire EM field, resulted in clear visualization of the position and form of each QD particle. When the corresponding EM image was overlaid, QDs could be readily differentiated from the grayscale cellular backgrounds (e.g., ribosomes) (Figure 2). Similar elemental mapping of Cd has been reported using electron energy loss spectrography (EELS) to detect QDs in ultrathin EM samples [35]. However, compared with EELS, EDX is more suitable for the detection of heavy metals, such as Cd or Se [19,36]. Moreover, because EELS is performed without electron staining, it is difficult to gain sufficient contrast in EM images [35]. Therefore, combined with pre-embedding Q-dot immunoEM and EDX mapping, the use of QDs is one of the most sensitive and distinct ultrastructural immunolabeling techniques available and might be particularly suitable for the correlation of LM/EM images.

Conclusions

Accurate identification of pretangles on LM, followed by EM examination of their exact counterpart was achieved through tau immunolabeling with QD, fluorescent nanocrystals, which are detectable with LM (fluorescence signal) and with EM (electron dense particles with halo). EDX spot analysis to confirm the identity of QD on EM section by showing energy peaks for Cd and Se is now extended to map the entire EM field to highlight QD particles. This improved method with EDX mapping clearly demonstrated for the first time that AD-pretangles showed a strong tendency to form fibrillary tangles even at an early stage, whereas pretangles or Pick-like inclusions in tissue from patients with CBD did not even at an advanced stage. This novel strategy is useful to clarify how molecules other than tau are organized into ultrastructures in the early stages of disease-specific lesions.

Additional files

Additional file 1: Figure S1. Optimal of dilution of QD-conjugated secondary antibodies for ultrastruc-tural immunolabeling.

Additional file 2: Figure S2. Energry dispersive X-ray (EDX) mapping of Quantum dots (QDs).

Competing interests

The authors declare that they have no competing interests.

Authors' contributions

ST, TU, RT and MY designed the study, analysed the data, and drafted the manuscript. ST, TU, IA, YI, MM, MY collected clinical and pathological data. All authors read and approved the final manuscript.

Acknowledgments

This study was supported by Grants-in-Aid for Scientific Research (JSPS KAKENHI 25430057) from the Ministry of Education, Culture, Sports, Science and Technology; a grant from the Japan Foundation for Neuroscience and Mental Health, the Mitsui Life Social Welfare Foundation, and the Tokyo Metropolitan Institute of Medical Science project 'Mechanism for Early Diagnosis and Prevention of Parkinson's disease; and Grants-in-Aid from the Research Committee of CNS Degenerative Diseases, the Ministry of Health, Labour and Welfare of Japan. We are grateful to Takashi Kanemura (Hitachi High-Technologies Corporation) for excellent operation of EDX spot analysis and mapping. Technical contributions by Mr. Kentaro Endo, Ms. Hiromi Kondo (Histology Center) and Ms. Ayako Nakamura (Laboratory of Structural Neuropathology) at Tokyo Metropolitan Institute of Medical Science are gratefully acknowledged.

Author details

[1]Department of Neuropathology, Institute for Medical Science of Aging, Aichi Medical University, Nagakute, Aichi, Japan. [2]Laboratory of Structural Neuropathology, Tokyo Metropolitan Institute of Medical Science, 2-1-6 Kamikitazawa, Setagaya, Tokyo 156-8506, Japan. [3]Department of Neurology, Kyoto University, Kyoto, Japan. [4]Department of Neurology, Higashi Nagoya National Hospital, Nagoya, Aichi, Japan.

Received: 5 November 2014 Accepted: 5 November 2014
Published online: 11 December 2014

References

1. Ross CA, Poirier MA (2004) Protein aggregation and neurodegenerative disease. Nat Med 10(Suppl):S10–S17, doi:10.1038/nm1066
2. Bancher C, Grundke-Iqbal I, Iqbal K, Fried VA, Smith HT, Wisniewski HM (1991) Abnormal phosphorylation of tau precedes ubiquitination in neurofibrillary pathology of Alzheimer disease. Brain Res 539(1):11–18
3. Braak E, Braak H, Mandelkow EM (1994) A sequence of cytoskeleton changes related to the formation of neurofibrillary tangles and neuropil threads. Acta Neuropathol 87(6):554–567
4. Uchihara T (2014) Pretangles and neurofibrillary changes -Similarities and differences between AD and CBD based on molecular and morphological evolution. Neuropathology 34(6):571–7, doi:10.1111/neup.12108
5. Kidd M (1963) Paired helical filaments in electron microscopy of Alzheimer's disease. Nature 197:192–193
6. Dickson DW, Bergeron C, Chin SS, Duyckaerts C, Horoupian D, Ikeda K, Jellinger K, Lantos PL, Lippa CF, Mirra SS, Tabaton M, Vonsattel JP, Wakabayashi K, Litvan I (2002) Office of Rare Diseases neuropathologic criteria for corticobasal degeneration. J Neuropathol Exp Neurol 61(11):935–946
7. Uchihara T, Mitani K, Mori H, Kondo H, Yamada M, Ikeda K (1994) Abnormal cytoskeletal pathology peculiar to corticobasal degeneration is different from that of Alzheimer's disease or progressive supranuclear palsy. Acta Neuropathol 88(4):379–383
8. Tatsumi S, Mimuro M, Iwasaki Y, Takahashi R, Kakita A, Takahashi H, Yoshida M (2014) Argyrophilic grains are reliable disease-specific features of corticobasal degeneration. J Neuropathol Exp Neurol 73(1):30–38, doi:10.1097/NEN.0000000000000022
9. Watanabe S, Punge A, Hollopeter G, Willig KI, Hobson RJ, Davis MW, Hell SW, Jorgensen EM (2011) Protein localization in electron micrographs using fluorescence nanoscopy. Nat Methods 8(1):80–84, doi:10.1038/nmeth.1537
10. Modla S, Czymmek KJ (2011) Correlative microscopy: a powerful tool for exploring neurological cells and tissues. Micron 42(8):773–792, doi:10.1016/j.micron.2011.07.001
11. Jahn KA, Barton DA, Kobayashi K, Ratinac KR, Overall RL, Braet F (2012) Correlative microscopy: providing new understanding in the biomedical and plant sciences. Micron 43(5):565–582, doi:10.1016/j.micron.2011.12.004
12. Caplan J, Niethammer M, Taylor RM 2nd, Czymmek KJ (2011) The power of correlative microscopy: multi-modal, multi-scale, multi-dimensional. Curr Opin Struct Biol 21(5):686–693, doi:10.1016/j.sbi.2011.06.010

13. Giepmans BN, Deerinck TJ, Smarr BL, Jones YZ, Ellisman MH (2005) Correlated light and electron microscopic imaging of multiple endogenous proteins using Quantum dots. Nat Methods 2(10):743–749, doi:10.1038/nmeth791
14. Karreman MA, Agronskaia AV, van Donselaar EG, Vocking K, Fereidouni F, Humbel BM, Verrips CT, Verkleij AJ, Gerritsen HC (2012) Optimizing immuno-labeling for correlative fluorescence and electron microscopy on a single specimen. J Struct Biol 180(2):382–386, doi:10.1016/j.jsb.2012.09.002
15. Deerinck TJ (2008) The application of fluorescent quantum dots to confocal, multiphoton, and electron microscopic imaging. Toxicol Pathol 36(1):112–116, doi:10.1177/0192623307310950
16. Cortese K, Diaspro A, Tacchetti C (2009) Advanced correlative light/electron microscopy: current methods and new developments using Tokuyasu cryosections. J Histochem Cytochem 57(12):1103–1112, doi:10.1369/jhc.2009.954214
17. Faas FG, Barcena M, Agronskaia AV, Gerritsen HC, Moscicka KB, Diebolder CA, van Driel LF, Limpens RW, Bos E, Ravelli RB, Koning RI, Koster AJ (2013) Localization of fluorescently labeled structures in frozen-hydrated samples using integrated light electron microscopy. J Struct Biol 181(3):283–290, doi:10.1016/j.jsb.2012.12.004
18. Heines MA, Guyot-Sionnest P (1996) Synthesis and characterization of strongly luminsecing ZnS-capped CdSe nanocrystals. J Phys Chem 100:468–471
19. Uematsu M, Adachi E, Nakamura A, Tsuchiya K, Uchihara T (2012) Atomic identification of fluorescent Q-dots on tau-positive fibrils in 3D-reconstructed pick bodies. Am J Pathol 180(4):1394–1397, doi:10.1016/j.ajpath.2011.12.029
20. Kanazawa T, Adachi E, Orimo S, Nakamura A, Mizusawa H, Uchihara T (2012) Pale neurites, premature alpha-synuclein aggregates with centripetal extension from axon collaterals. Brain Pathol 22(1):67–78, doi:10.1111/j.1750-3639.2011.00509.x
21. Montine TJ, Phelps CH, Beach TG, Bigio EH, Cairns NJ, Dickson DW, Duyckaerts C, Frosch MP, Masliah E, Mirra SS, Nelson PT, Schneider JA, Thal DR, Trojanowski JQ, Vinters HV, Hyman BT (2012) National Institute on Aging-Alzheimer's Association guidelines for the neuropathologic assessment of Alzheimer's disease: a practical approach. Acta Neuropathol 123(1):1–11, doi:10.1007/s00401-011-0910-3
22. Takahashi T, Amano N, Hanihara T, Nagatomo H, Yagishita S, Itoh Y, Yamaoka K, Toda H, Tanabe T (1996) Corticobasal degeneration: widespread argentophilic threads and glia in addition to neurofibrillary tangles. Similarities of cytoskeletal abnormalities in corticobasal degeneration and progressive supranuclear palsy. J Neurol Sci 138(1–2):66–77
23. Arima K, Uesugi H, Fujita I, Sakurai Y, Oyanagi S, Andoh S, Izumiyama Y, Inose T (1994) Corticonigral degeneration with neuronal achromasia presenting with primary progressive aphasia: ultrastructural and immunocytochemical studies. J Neurol Sci 127(2):186–197
24. Feany MB, Dickson DW (1995) Widespread cytoskeletal pathology characterizes corticobasal degeneration. Am J Pathol 146(6):1388–1396
25. Ksiezak-Reding H, Morgan K, Mattiace LA, Davies P, Liu WK, Yen SH, Weidenheim K, Dickson DW (1994) Ultrastructure and biochemical composition of paired helical filaments in corticobasal degeneration. Am J Pathol 145(6):1496–1508
26. Mori H, Nishimura M, Namba Y, Oda M (1994) Corticobasal degeneration: a disease with widespread appearance of abnormal tau and neurofibrillary tangles, and its relation to progressive supranuclear palsy. Acta Neuropathol 88(2):113–121
27. Lippa CF, Smith TW, Fontneau N (1990) Corticonigral degeneration with neuronal achromasia. A clinicopathologic study of two cases. J Neurol Sci 98(2–3):301–310
28. Wakabayashi K, Oyanagi K, Makifuchi T, Ikuta F, Homma A, Homma Y, Horikawa Y, Tokiguchi S (1994) Corticobasal degeneration: etiopathological significance of the cytoskeletal alterations. Acta Neuropathol 87(6):545–553
29. Kato S, Nakamura H, Otomo E (1989) Reappraisal of neurofibrillary tangles. Immunohistochemical, ultrastructural, and immunoelectron microscopical studies. Acta Neuropathol 77(3):258–266
30. Lowe J, Mirra SS, Hyman B, Dickson DW (2008) Histopathology of Alzheimer's disease. In: Love S, Louis DN, Ellison DW (eds) Greenfield's neuropathology, vol 1, 8th edn. Edward Arnold, London, pp 1031–1152
31. Metuzals J, Robitaille Y, Houghton S, Gauthier S, Leblanc R (1988) Paired helical filaments and the cytoplasmic-nuclear interface in Alzheimer's disease. J Neurocytol 17(6):827–833
32. Hara M, Hirokawa K, Kamei S, Uchihara T (2013) Isoform transition from four-repeat to three-repeat tau underlies dendrosomatic and regional progression of neurofibrillary pathology. Acta Neuropathol 125(4):565–579, doi:10.1007/s00401-013-1097-6
33. Andorfer C, Acker CM, Kress Y, Hof PR, Duff K, Davies P (2005) Cell-cycle reentry and cell death in transgenic mice expressing nonmutant human tau isoforms. J Neurosci 25(22):5446–5454, doi:10.1523/JNEUROSCI. 4637-04.2005
34. Yang Y, Geldmacher DS, Herrup K (2001) DNA replication precedes neuronal cell death in Alzheimer's disease. J Neurosci 21(8):2661–2668
35. Nisman R, Dellaire G, Ren Y, Li R, Bazett-Jones DP (2004) Application of quantum dots as probes for correlative fluorescence, conventional, and energy-filtered transmission electron microscopy. J Histochem Cytochem 52(1):13–18
36. Leapman RD, Ornberg RL (1988) Quantitative electron energy loss spectroscopy in biology. Ultramicroscopy 24(2–3):251–268

doi:10.1186/s40478-014-0161-3
Cite this article as: Tatsumi *et al.*: Ultrastructural differences in pretangles between Alzheimer disease and corticobasal degeneration revealed by comparative light and electron microscopy. *Acta Neuropathologica Communications* 2014 2:161.

RESEARCH PAPER

A nationwide survey of hypertrophic pachymeningitis in Japan

Tomomi Yonekawa,[1] Hiroyuki Murai,[1] Satoshi Utsuki,[2] Takuya Matsushita,[1] Katsuhisa Masaki,[1] Noriko Isobe,[1] Ryo Yamasaki,[3] Mari Yoshida,[4] Susumu Kusunoki,[5] Kiyomi Sakata,[6] Kiyotaka Fujii,[2] Jun-ichi Kira[1]

▶ Additional material is published online only. To view please visit the journal online (http://dx.doi.org/10.1136/jnnp-2013-306410).

[1]Department of Neurology, Neurological Institute, Graduate School of Medical Sciences, Kyushu University, Fukuoka, Japan
[2]Department of Neurosurgery, Kitasato University School of Medicine, Sagamihara, Japan
[3]Department of Neurological Therapeutics, Neurological Institute, Graduate School of Medical Sciences, Kyushu University, Fukuoka, Japan
[4]Department of Neuropathology, Institute for Medical Science of Aging, Aichi Medical University, Nagakute, Japan
[5]Department of Neurology, School of Medicine, Kinki University, Osaka, Japan
[6]Department of Hygiene and Preventive Medicine, Iwate Medical University School of Medicine, Morioka, Japan

Correspondence to
Professor Jun-ichi Kira, Department of Neurology, Neurological Institute, Graduate School of Medical Sciences, Kyushu University, 3-1-1 Maidashi, Higashi-ku, Fukuoka 812-8582, Japan; kira@neuro.med.kyushu-u.ac.jp

Received 26 July 2013
Revised 25 October 2013
Accepted 3 November 2013
Published Online First 22 November 2013

To cite: Yonekawa T, Murai H, Utsuki S, *et al*. *J Neurol Neurosurg Psychiatry* 2014;**85**: 732–739.

ABSTRACT

Objectives To clarify the prevalence, frequent causes and distinct features of hypertrophic pachymeningitis (HP) according to background conditions in a nationwide survey in Japan.

Methods The study began with a preliminary survey to determine the approximate number of HP patients diagnosed from 1 January 2005 to 31 December 2009, and was followed by a questionnaire survey for clinical and laboratory findings. HP was defined as a condition with thickening of the cranial or spinal dura mater with inflammation, evidenced by MRI or histology.

Results Crude HP prevalence was 0.949/100 000 population. The mean age at onset was 58.3±15.8 years. Among 159 cases for whom detailed data were collated, antineutrophil cytoplasmic antibody (ANCA)-related HP was found in 54 cases (34.0%) and IgG4/multifocal fibrosclerosis (MFS)-related HP in 14 cases (8.8%). Seventy cases (44.0%) were classified as 'idiopathic' and 21 (13.2%) as 'others'. ANCA-related HP cases showed a female preponderance, a higher age of onset, and higher frequencies of otological symptoms and elevated systemic inflammatory biomarkers, but lower frequencies of diplopia compared with idiopathic HP. IgG4/MFS-related HP cases showed a marked male predominance; all had cranial HP while none had isolated spinal HP or decreased sensation.

Conclusions HP is not extremely rare. ANCA-related HP is the most frequent form, followed by IgG4/MFS-related HP. Both forms have unique features, which may help to differentiate background causes.

INTRODUCTION

Cranial and spinal hypertrophic pachymeningitis (HP) is a rare inflammatory disorder demonstrating local or diffuse thickening of the intracranial or spinal dura mater. Thickening of the dura mater causes intracranial hypertension, cranial nerve palsy and spinal cord dysfunction. MRI findings show thickening and contrast enhancement of the affected dura mater. HP pathology shows interstitial fibrosis and inflammatory cell infiltration consisting mainly of lymphocytes. HP is aetiologically heterogeneous, secondarily developing in association with a variety of conditions, such as infection, autoimmune disease, trauma and tumours, or being labelled idiopathic in the absence of an identifiable cause.[1 2] The mechanisms underlying idiopathic HP are thus ill defined, and unidentified causes might exist. Because there have been no epidemiological or large-scale clinical studies of HP, its prevalence, frequent causes and distinct features according to background conditions are totally unknown. Therefore, we aimed to clarify these issues in a nationwide survey of HP in Japan.

METHODS

Procedures

The nationwide survey was conducted by the Research Committee of HP, sponsored by the Ministry of Health, Labour and Welfare, Japan. This study was approved by the Kyushu University Ethics Committee. The survey was undertaken in two steps: first, a preliminary survey to ascertain the approximate number of HP patients in Japan, and second, a survey using a questionnaire sheet for each patient. The hospitals studied were randomly selected from the directory of all registered hospitals in Japan. Selection was made according to stratification based on the number of beds in each hospital; the more beds a hospital had, the higher its probability of being selected.[3] HP was defined as a thickening of the cranial or spinal dura mater with inflammation, and cases in whom either thickening of the dura mater was detected by MRI, or fibrotic thickening with inflammatory cell infiltration was observed in biopsied dura mater, were included. We excluded cases associated with malignancy and intracranial hypotension.

The questionnaire for the preliminary survey on HP patients who, because of the disease, visited hospitals from 1 January 2005 to 31 December 2009 was mailed to 5477 hospital departments (446 neurology, 731 neurosurgery, 994 internal medicine, 951 orthopaedics, 770 otorhinolaryngology, 800 paediatrics and 785 ophthalmology departments) together with the inclusion criteria. Following the collection and collation of the results of the first questionnaire, the second questionnaire was forwarded to those reporting patients in the first survey. It requested detailed clinical information on individual patients including age at onset and examination, sex, symptoms based on history and signs based on neurological examination, coexisting diseases, laboratory findings, MRI findings of brain and spinal cords, pathological findings, clinical course, treatment and prognosis. Patients reported by more than one hospital or department were treated as duplicate.

Laboratory findings included myeloperoxidase (MPO)- and proteinase-3 (PR3)-antineutrophil cytoplasmic antibody (ANCA) positivity, and elevation of

IgG4. We further classified cases into several categories according to positive findings for ANCA, IgG4 elevation and coexisting diseases. Patients were regarded as having ANCA-related HP if either MPO-ANCA or PR3-ANCA was detected, or ANCA-related diseases (ANCA-related angiitis or Wegener's granulomatosis) coexisted. Diagnosis of IgG4/multifocal fibrosclerosis (MFS)-related HP was based on the established criteria for IgG4-related disease[4] (clinical examination showing characteristic diffuse/local swelling or mass in single or multiple organs, elevated serum IgG4 levels >135 mg/dL, and IgG4-positive plasma cells in the biopsied dura with a IgG4-positive/IgG-positive cell ratio >40% and more than 10 IgG4+ plasma cells per high-power field), or the presence of MFS, such as retroperitoneal fibrosis, mediastinal fibrosis, sclerosing pancreatitis, Riedel's thyroiditis and pseudotumour of the orbit. Idiopathic HP comprised cases with no evidence of ANCA- or IgG4/MFS-related conditions, or without other causes including relevant infections asked about in the second survey, such as syphilis, tuberculosis, fungal infections (candidiasis, aspergillosis), bacterial infections (*Pseudomonas aeruginosa*, *Propionibacterium acnes*), borreliosis and cysticercosis.

Statistical analysis

The estimated total number of HP patients in Japan was extrapolated from our data using formulae derived by the epidemiology committee,[3 5] taking response rates into account. First, for each stratum, the total reported number of patients was divided by the ratio of responding institutions to the number of surveyed institutions. The results for all strata were then added to estimate the total number of HP patients.[5] Statistical analyses of numerical variables were initially performed using the Pearson's χ^2 test and Kruskal–Wallis test. When statistical significance was found, Pearson's χ^2 test or Fisher's exact test was used to determine the statistical significance of differences between groups. Uncorrelated p values were corrected by multiplying them by the number of comparisons (Bonferroni–Dunn's correction) to calculate corrected p values. Differences in ratios between two groups were tested for significance by the χ^2 test or Fisher's exact test when the criteria for the χ^2 tests were not fulfilled. In all assays, p values <0.05 were considered statistically significant.

RESULTS

Baseline characteristics

In the preliminary survey, 1904 departments (34.8%) responded, reporting 324 HP patients. In the second questionnaire, detailed clinical data on 159 patients (49.1% of those reported in the preliminary survey) were collected. The estimated crude prevalence was 0.949/100 000 population (95% CI 0.833 to 1.065). The male to female ratio was 1:0.91 (table 1). The mean age at onset was 58.3±15.8 years, and mean age at first visit to the physician was 59.7±15.2 years. HP diagnosis was made by MRI alone in 106 cases, MRI and pathology in 49 cases, and pathology alone in four cases.

Table 1 Demographic features of the 159 patients with hypertrophic pachymeningitis

Basic demographics		Initial symptoms	Number (%)
Number of cases analysed	159	Headache	56 (35.2)
Sex ratio (male:female)	1:0.91	Visual loss	21 (13.2)
Age at onset (mean±SD, years)	58.3±15.8	Double vision	20 (12.6)
Age at first visit to physician (mean±SD, years)	59.7±15.2	Otological symptoms	15 (9.4)
Disease duration (mean±SD, months)	48.3±50.9	Symptoms during entire course	Number (%)
Underlying diseases	Number	Headache	113 (71.1)
ANCA-related angiitis	21	Back pain	6 (3.8)
Wegener's granulomatosis	19	Fever	42 (26.4)
Multifocal fibrosclerosis	6*	Consciousness disturbance	21 (13.2)
IgG4-related disease	9	Convulsion	14 (8.8)
Otitis media	3	Memory disturbance and other higher brain dysfunction	11 (6.9)
Cholesteatoma of the middle ear	1	Visual loss	52 (32.7)
Sinusitis	1	Double vision	46 (28.9)
Sjögren syndrome	2	Dysphagia	13 (8.2)
Tuberculosis	2	Dysarthria	11 (6.9)
Aspergillosis	2	Weakness (facial and/or extremities)	38 (23.9)
Site of dural hypertrophy	Number (%)	Sensory disturbance	45 (28.3)
Cranial	135 (84.9)	Bladder disturbance	10 (6.3)
Spinal	14 (8.8)	Bowel disturbance	7 (4.4)
Cranial and spinal	7 (4.4)	Neurological findings	Number (%)
Mode of onset	Number (%)	Cranial nerve palsy	99 (62.3)
Acute	41 (25.8)	Neck stiffness	7 (4.4)
Subacute	75 (47.2)	Motor impairment	26 (16.4)
Chronic	27 (17.0)	Abnormal tendon reflexes	44 (27.7)
Clinical course	Number (%)	Pathological reflexes	15 (9.4)
Monophasic	51 (32.1)	Limb and/or truncal ataxia	6 (3.8)
Progressive	28 (17.6)	Decreased sensation	31 (19.5)
Relapsing-remitting	62 (39.0)	Sphincter dysfunction	5 (3.1)
Unknown	18 (11.3)		

*Includes five cases of MFS-related HP and one case assigned to ANCA-related HP.
ANCA, antineutrophil cytoplasmic antibody; HP, hypertrophic pachymeningitis; MFS, multifocal fibrosclerosis.

Table 2 Cranial nerve involvement in hypertrophic pachymeningitis patients

	n/N (%)
Cranial nerve involvement	99/159 (62.3)
Single	40/99 (40.4)
Multiple	59/99 (59.6)
Cranial nerves	n/N (%)
I	2/99 (2.0)
II	41/99 (41.4)
III	30/99 (30.3)
IV	25/99 (25.3)
V	19/99 (19.2)
VI	35/99 (35.4)
VII	19/99 (19.2)
VIII	27/99 (27.3)
IX	13/99 (13.1)
X	10/99 (10.1)
XI	5/99 (5.1)
XII	8/99 (8.1)

n, number of involved cases, N, number of cases collated, or total number of involved cases.

The diseases underlying HP were heterogeneous. ANCA-related angiitis and Wegener's granulomatosis were the most common coexisting diseases. IgG4/MFS-related diseases followed. Among 14 cases diagnosed as having IgG4/MFS-related HP, four cases had retroperitoneal fibrosis and were thus regarded as having MFS-related HP. The remaining 10 cases were diagnosed as having IgG4-related HP based on the IgG4-related disease criteria[4]; one had definite IgG4-related disease (IgG4+ cells in biopsied dura, elevated serum IgG4 concentrations and diffuse/local organ swelling or mass), six of these had probable IgG4-related HP (IgG4+ cells in biopsied dura and diffuse/local organ swelling or mass), and three had possible IgG4-related HP (elevated serum IgG4 concentrations and diffuse/local organ swelling or mass). Otorhinolaryngological disorders, such as otitis media and sinusitis, occasionally accompanied. Infectious causes were rarely identified, with only two cases with tuberculosis and two cases of aspergillosis. HP was confined to the cranial dura in 137 cases (86.2%), the spinal dura in 15 (9.4%), and both in 7 (4.4%) (demographic features according to the sites of HP are shown in online supplementary table S1). Approximately half the HP cases had subacute onset, whereas, the rest showed either an acute or chronic pattern. More than 50% of HP patients showed either a relapsing-remitting or progressive course.

Symptoms and neurological findings

Headache was the most common initial symptom of HP (35.2%), followed by ophthalmological symptoms, such as visual loss and double vision (each 13.2% and 12.6%, respectively) (table 1). Some patients (9.4%) had otological symptoms including deafness and tinnitus. During the entire course, the frequency of headache rose to 71.1%. Fever was seen in one-quarter of HP patients. Visual loss and double vision were observed in approximately one-third of HP patients, compared with <10% for dysphagia and dysarthria. Neurological findings revealed frequent involvement of the cranial nerves (62.3%). Multiple involvements were more common than isolated involvement, and cranial nerves II–VIII were more frequently affected than IX–XII (table 2). Although headache was the most frequent symptom, neck stiffness was uncommon (4.4%). Abnormal tendon reflex and decreased sensation were seen in approximately one-quarter of HP patients. Ataxia and sphincter dysfunction were relatively rare.

Laboratory findings in peripheral blood and CSF

Non-specific inflammation was seen in a half to three-quarters of HP cases, such as increased erythrocyte sedimentation rate (ESR), white blood cells (WBC) or C-reactive protein (CRP) (table 3). Antinuclear antibody was detected in 16.9% of cases

Table 3 Laboratory, neuroimaging, and pathological findings in 159 hypertrophic pachymeningitis cases

Laboratory findings	n/N (%)	Neuroimaging	n/N (%)
Blood		MRI	
ESR elevation	78/104 (75.0)	Thickening of the cranial dura mater	141/156 (90.4)
WBC increase	63/146 (43.2)	Gd enhancement of cranial dura	124/139 (89.2)
CRP elevation	110/149 (73.8)	Thickening of the spinal dura mater	21/54 (38.9)
ANA elevation	20/118 (16.9)	Gd enhancement of spinal dura	17/20 (85.0)
MPO-ANCA positivity	33/119 (27.7)	Gallium scintigraphy	
PR3-ANCA positivity	14/111 (12.6)	Increased uptake	22/50 (44.0)
IgG4 elevation	7/27 (25.9)	SPECT	
STS	2/122 (1.6)	Hypoperfusion	7/29 (24.1)
Anti-HTLV-1 Ab	1/50 (2.0)	Hyperperfusion	3/29 (10.3)
ADA elevation	3/28 (10.7)	PET	
ACE elevation	1/56 (1.8)	Positive accumulation	2/17 (11.8)
CSF		Pathological findings of dura mater	n/N (%)
Pleocytosis	71/116 (61.2)	Fibrosis	43/52 (82.7)
Protein elevation	115/119 (99.6)	Infiltration of inflammatory cells	47/52 (90.4)
TPLA positivity	0/7 (0.0)	Angiitis	4/52 (7.7)
ADA elevation	2/22 (9.1)	Granuloma	15/52 (28.8)
		Necrosis	8/52 (15.4)
		Oedema	5/52 (9.6)
		IgG4-positive plasma cells	11/42 (26.2)

Ab, antibody; ADA, adenosine deaminase; ANA, antinuclear antibody; CRP, C-reactive protein; CSF, cerebrospinal fluid; ESR, erythrocyte sedimentation rate; Gd, gadolinium; HTLV-1, human T-lymphotrophic virus type I; MPO-ANCA, myeloperoxidase-antineutrophil cytoplasmic antibodies; PET, positron emission tomography; PR3-ANCA, proteinase-3-antineutrophil cytoplasmic antibodies; SPECT, single photon emission CT; STS, serologic test for syphilis; TPLA, treponema pallidum latex agglutination; WBC, white blood cells.

assessed, and adenosine deaminase (ADA) was elevated in 10.7%. Serologic tests for syphilis and human T-lymphotrophic virus type 1 antibody were rarely positive (1.6% and 2.0%, respectively). The most noticeable finding was that MPO-ANCA and PR3-ANCA were positive in 33/119 (27.7%) and 14/111 (12.6%) cases assessed, respectively. In four cases, MPO-ANCA and PR3-ANCA were detected. As a result, 43 cases were ANCA-positive. Furthermore, hyper-IgG4aemia was observed in 7/27 (25.9%) cases examined. Cerebrospinal fluid (CSF) pleocytosis was detected in 71/116 (61.2%) cases, while variable degrees of protein elevation were found in 115/116 (96.6%) cases. ADA elevation in the CSF was found in 2/22 (9.1%) cases.

Neuroimaging

On brain MRI, hypertrophic change of the cranial dura mater was found in 141/156 (90.4%) cases examined (table 3). Gadolinium (Gd) enhancement was observed in 124/139 (89.2%). Hypertrophic changes of the spinal dura mater were found in 21/54 (38.9%) cases examined, while Gd-enhancement was seen in 17/20 (85.0%). Thickening of the cranial dura mater was diffuse in 33/141 (23.4%) cases and partial in 108/141 (76.6%). Increased uptake in gallium scintigraphy was found in 22/50 (44.0%). Abnormalities in single photon emission CT (SPECT) and positron emission tomography (PET) findings were observed in 10/29 (34.5%) cases and 2/17 (11.8%) cases, respectively.

Pathological findings

Fifty-two patients underwent biopsy of the dura mater (table 3). The main pathological findings were fibrosis (82.7%), inflammatory cell infiltration (monocytes, plasma cells, eosinophils and polymorphonuclear leucocytes) (90.4%) and granuloma (28.8%). Necrosis and oedema were found in some cases. Importantly, IgG4-positive cells were found in 11/42 (26.2%) cases assessed; seven in IgG4/MFS-related HP and four in ANCA-related HP. Importantly, IgG4-positive cells were found in 11/42 (26.2%) cases assessed. Angiitis was detected in 4/52 cases (7.7%). Culture of the biopsied dura mater in 27 patients identified tuberculosis in one while the rest were negative. The brain adjacent to thickened dura mater was biopsied in eight cases, revealing infiltration of inflammatory cells in seven, while granuloma and necrosis were each observed in four cases, and IgG4-positive cells in one.

Treatment

Selected treatment options in our HP series are listed in online supplementary table S2. In 12 cases of infectious HP, antibiotic, antifungal, and antituberculosis drugs were used as the first-line therapy for relevant pathogens. Corticosteroids, mostly methylprednisolone pulse therapy followed by oral administration, were administered as the first choice for HP when infectious cases were excluded. A total of 94 cases received corticosteroids as immunotherapy at first, resulting in an 87.2% improvement. In 54 cases with insufficient response to corticosteroids, immunosuppressants were added and 92.6% improved. Only 24 cases (15.1%) required surgery.

Comparison of idiopathic, ANCA-related and IgG4/MFS-related HP

According to the classification stated in the section on Methods, ANCA-related and IgG4/MFS-related diseases are the two major causes of HP in Japan (figure 1A,B). There were 48 (30.2%) and 14 (8.8%) cases of ANCA-related and IgG4/MFS-related HP, respectively. Six patients (3.8%) with ANCA-related HP also had either hyper-IgG4aemia or IgG4-positive plasma cells in the biopsied dura (combined cases in figure 1A,B). Such cases were included in the ANCA-related HP group in the following analyses because they showed similar features to ANCA-related HP and ANCA-related disease could show hyper-IgG4aemia. Idiopathic HP comprised 44.0% (70/159) of cases while various other causes were responsible for 13.2% (21/159).

Comparisons of demographic features among idiopathic, ANCA-related and IgG4/MFS-related HP revealed a male predominance for idiopathic HP (male:female=1:0.75) and a female preponderance for ANCA-related HP (1:1.34) (table 4). Interestingly, IgG4/MFS-related HP showed a marked male predominance (1:0.17). Thus, sex ratios were significantly different among the three groups. All IgG4/MFS-related HP cases exhibited cranial HP; none showed isolated spinal HP, while isolated spinal HP was occasionally seen in idiopathic and ANCA-related HP (12.9% and 5.6%, respectively). Age of onset was significantly older in ANCA-related HP cases than in idiopathic HP cases. There was no significant difference in the mode of onset and clinical course among the three groups; however, ANCA-related HP cases less frequently developed acute onset while IgG4/MFS-related HP cases tended to show a monophasic course more frequently than did the others ($p=0.0553$).

As initial symptoms, ANCA-related HP cases showed a higher frequency of otological symptoms but lower frequency of double vision, compared with idiopathic HP cases (see table 4 and online supplementary figure S1). Regarding symptoms and signs during the entire course, ANCA-related HP cases had significantly greater frequency of fever compared with idiopathic HP, and lower frequency of double vision compared with idiopathic and IgG4/MFS-related HP cases. Sensory disturbance was more common in idiopathic HP cases than ANCA-related and IgG4/MFS-related HP cases. Systemic inflammatory responses, such as elevated ESR and CRP, and increased WBC, were more frequently found in ANCA-related HP compared with idiopathic HP.

DISCUSSION

This nationwide epidemiological survey of HP in Japan enabled us to elucidate the prevalence and clinical characteristics of HP. This is epoch-making because there has been no previous epidemiological survey of HP, with a series of approximately 10 patients being the largest.[1 6] The main new findings of the present study are as follows: (1) crude HP prevalence was determined to be 0.949/100 000; (2) among all HP cases, the most common cause is ANCA-related HP, making up as much as 34.0% of all cases, and the second most common cause is IgG4/MFS-related HP, making up 8.8% (12.6%, if including ANCA-related HP cases with hyper-IgG4aemia); (3) ANCA-related HP showed a female preponderance, a higher age at onset, and higher frequencies of otological symptoms and elevated systemic inflammatory markers compared with idiopathic HP, but lower frequencies of diplopia compared with idiopathic and IgG4/MFS-related HP; (4) IgG4/MFS-related HP showed a marked male predominance, and all IgG4/MFS-related HP patients had cranial HP while none had isolated spinal HP, resulting in a lower frequency of decreased sensation compared with idiopathic HP patients who occasionally had spinal HP.

However, our study has some limitations. First, the rate of response to the preliminary survey was not very high; however, the estimated number of HP patients in Japan was calculated by taking the response rate in each stratum into account.[5] The response rate in the secondary survey was reasonably high

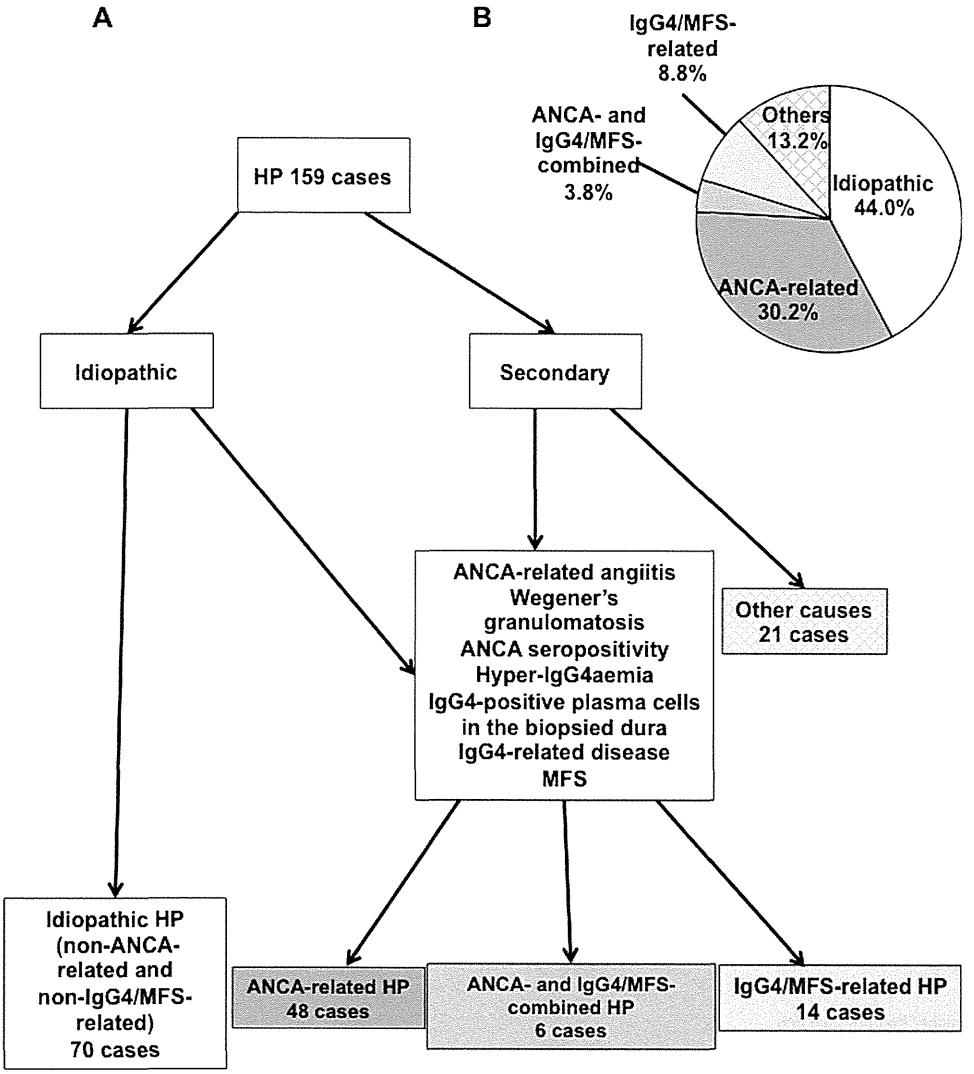

Figure 1 Classification of hypertrophic pachymeningitis (HP) in the present nationwide survey in Japan. (A) Flow chart showing the classification of the 159 HP patients. Causes of HP, idiopathic or secondary, were initially judged by the physician in charge. We classified 70 cases as having idiopathic HP because neither antineutrophil cytoplasmic antibody (ANCA)-related nor IgG4/multifocal fibrosclerosis (MFS)-related systemic diseases was present. We extracted 68 cases with ANCA-related angiitis, Wegener's granulomatosis, ANCA-seropositivity, hyper-IgG4aemia, IgG4-positive plasma cells in the biopsied dura mater, IgG4-related disease, and MFS from cases with secondary HP and those initially judged as 'idiopathic HP' by the physician in charge. We further divided them into 48 cases with ANCA-related HP, 14 cases with IgG4/MFS-related HP, and six cases with combined ANCA-related and IgG4/MFS-related HP. (B) Proportions of idiopathic and secondary HP according to the major underlying diseases. Idiopathic HP accounts for 44.0% of all cases while ANCA-related and IgG4/MFS-related cases make up 30.2% and 8.8%, respectively. When ANCA- and IgG4/MFS-combined cases (3.8%) are included, the percentages rise to 34.0% in ANCA-related HP and 12.6% in IgG4/MFS-related HP.

compared with the response rates of the secondary surveys in recent nationwide epidemiological surveys of multiple sclerosis and myasthenia gravis conducted in Japan (39.3% and 36.9%, respectively).[3 7] We thus believe that the response rates did not impair the quality of the present study. Second, the diagnosis of HP depended on a decision by a doctor in charge, and we cannot completely neglect the possibility that the doctors in charge did not have an opportunity to thoroughly review the medical charts and radiological reports. ANCA and serum IgG4 were not examined in all patients, generating a possibility that the idiopathic HP group may contain some secondary HP cases. Third, therapeutic efficacy was based on the judgement of each doctor, yielding some uncertainty. Fourth, performance of Gd-enhanced MRI was not an inclusion criterion, which may have caused some diagnostic inaccuracy in 11 patients (6.9%) diagnosed with non-enhanced MRI alone in the second survey. With these reservations in mind, the prevalence of HP in Japan (0.949/100 000) is much higher than those of rare neurological diseases, such as Creutzfeldt–Jakob disease (0.1/100 000).[8] Given the relapsing and progressive nature of HP without adequate medication, it casts a non-negligible healthcare burden on our society.

The most important finding of the present study is that ANCA-related disease and IgG4/MFS-related disease are the two major conditions underlying HP in Japan, where infectious causes are infrequent. Both conditions may not be mutually exclusive, and indeed, occurrence of IgG4-related HP was previously reported in association with either ANCA positivity[9] or Churg–Strauss syndrome (CSS).[10] However, because CSS itself shows hyper-IgG4aemia,[11] increased serum IgG4 levels in ANCA-related HP may not be pathognomonic. Wegener's granulomatosis frequently produces mucosal thickening of the nasal

Table 4 Comparison of clinical features among idiopathic, ANCA-related, and IgG4/MFS-related hypertrophic pachymeningitis cases

	Idiopathic n=70	ANCA-related n=54	IgG4/MFS-related n=14	p Value
Sex ratio (male:female)	1:0.75	1:1.34	1:0.17	**0.0126***
Location of hypertrophic dura				
Cranial	58 (82.9)	49 (90.7)	14 (100.0)	NS
Spinal	9 (12.9)	3 (5.6)	0 (0.0)	NS
Cranial and spinal	3 (4.3)	2 (3.7)	0 (0.0)	NS
Age of onset (mean±SD, years)	54.8±16.5	62.5±14.4	56.7±12.5	**0.0183†**
Time between onset and diagnosis (mean±SD, months)	25.3±72.2	14.6±36.6	3.57±3.59	NS
Age at first visit to physician (mean±SD, years)	56.4±16.0	63.5±13.6	57.0±12.5	**0.0321†**
Disease duration (mean±SD, months)	49.8±52.7	49.3±51.8	20.3±20.7	NS
Mode of onset				
Acute	21 (30.0)	12 (22.2)	5 (35.7)	NS
Subacute	29 (41.4)	28 (51.9)	8 (57.1)	NS
Chronic	16 (22.9)	7 (13.0)	1 (7.1)	NS
Unknown	4 (5.7)	7 (13.0)	0 (0.0)	
Clinical course				
Monophasic	23 (32.9)	16 (29.6)	9 (64.3)	NS
Progressive	14 (20.0)	8 (14.8)	2 (14.3)	NS
Relapsing-remitting	27 (38.6)	22 (40.7)	3 (21.4)	NS
Unknown	6 (8.6)	8 (14.8)	0 (0.0)	
Initial symptom				
Headache	22 (31.4)	14 (25.9)	7 (50.0)	NS
Visual loss	12 (17.1)	3 (5.6)	1 (7.1)	NS
Double vision	14 (20.0)	2 (3.7)	3 (21.4)	**0.0387†**
Otological symptoms	3 (4.3)	12 (22.2)	1 (7.1)	**0.0124†**
Symptoms and signs during entire course				
Headache	44 (62.9)	43 (79.6)	11 (78.6)	NS
Back pain	6 (8.6)	0 (0.0)	0 (0.0)	NS
Fever	11 (15.7)	25 (46.3)	2 (14.3)	**<0.001†**
Consciousness disturbance	10 (14.3)	7 (13.0)	3 (21.4)	NS
Convulsion	7 (10.0)	6 (11.1)	1 (7.1)	NS
Memory disturbance /higher brain dysfunction	5 (7.1)	5 (9.3)	1 (7.1)	NS
Visual loss	21 (30.0)	14 (25.9)	3 (21.4)	NS
Double vision	26 (37.1)	8 (14.8)	7 (50.0)	**0.0236†, 0.0149***
Dysphagia	6 (8.6)	4 (7.4)	1 (7.1)	NS
Dysarthria	5 (7.1)	4 (7.4)	0 (0.0)	NS
Weakness (facial and/or extremities)	22 (31.4)	11 (20.4)	1 (7.1)	NS
Sensory disturbance	29 (41.4)	10 (18.5)	1 (7.1)	**0.0321†**
Bladder disturbance	6 (8.6)	2 (3.7)	0 (0.0)	NS
Bowel disturbance	4 (5.7)	2 (3.7)	0 (0.0)	NS
Neurological findings				
Cranial nerve palsy	39 (55.7)	34 (63.0)	10 (71.4)	NS
Neck stiffness	3 (4.3)	2 (3.7)	2 (14.3)	NS
Motor impairment	14 (20.0)	8 (14.8)	1 (7.1)	NS
Abnormal tendon reflexes	20 (28.6)	17 (31.5)	0 (0.0)	NS
Pathological reflexes	8 (11.4)	4 (7.4)	0 (0.0)	NS
Limb and/or truncal ataxia	3 (4.3)	2 (3.7)	0 (0.0)	NS
Decreased sensation	24 (34.3)	12 (22.2)	0 (0.0)	NS
Sphincter dysfunctions	6 (8.6)	2 (3.7)	0 (0.0)	NS
Laboratory data				
WBC increase	17 (24.3)	34 (63.0)	6 (42.9)	**<0.001†**
ESR elevation	27 (38.6)	34 (63.0)	8 (57.1)	**0.0219†**
CRP elevation	38 (54.3)	47 (87.0)	12 (85.7)	**<0.001†**
Reaction to immunotherapy				
Corticosteroids				
Remission	27/46 (58.7)	7/12 (58.3)	7/13 (53.8)	NS
Insufficient	15/46 (32.6)	4/12 (33.3)	4/13 (30.8)	NS
Unknown	4/46 (8.7)	1/12 (8.3)	2/13 (15.4)	

Continued

Table 4 Continued

	Idiopathic n=70	ANCA-related n=54	IgG4/MFS-related n=14	p Value
Corticosteroids+immunosuppressants				
Remission	3/14 (21.4)	12/28 (42.9)	0/1 (0.0)	NS
Insufficient	9/14 (64.3)	12/28 (42.9)	1/1 (100.0)	NS
Unknown	2/14 (14.3)	4/28 (14.3)	0/1 (0.0)	

A p value of <0.05 has been estimated as significant among the three groups because we performed Bonferroni-Dunn's correction. When we found a significant difference among the three groups, we performed a Mann–Whitney's test, Pearson's χ^2 test or Fisher's exact test to assess the significance of differences between groups.
†Between idiopathic and ANCA-related HP.
*Between ANCA-related and IgG4/MFS-related HP.
Concerning the clinical features according to the location of hypertrophic dura, see the online supplementary table S1.
ANCA, antineutrophil cytoplasmic antibody; CRP, C-reactive protein; ESR, erythrocyte sedimentation rate; HP, hypertrophic pachymeningitis; MFS, multifocal fibrosclerosis; WBC, white blood cells.

and paranasal sinuses[12]; therefore, its intracranial extension could produce HP. There are several reports of HP harbouring ANCA in the absence of clinically overt manifestations of Wegener's granulomatosis.[13–15] We included HP cases demonstrating ANCA positivity alone in the ANCA-related HP group, because demographic features are similar between those with and without clinical manifestations of Wegener's granulomatosis.

Based on the observation that HP developed in a patient with MFS,[16] a chronic fibrosing inflammation of connective tissues comprising retroperitoneal and mediastinal fibrosis, sclerosing pancreatitis and cholangitis, and Riedel's thyroiditis,[17] it was proposed that HP could be a manifestation of MFS. Later, with the finding of infiltration of IgG4-positive plasma cells and hyper-IgG4aemia in lymphoplasmacytic sclerosing pancreatitis, cholangitis, sialadenitis and retroperitoneal fibrosis, MFS was supposed to be an IgG4-related disease, featuring IgG4-positive plasma cell infiltration and fibrosis in many organs.[18 19] Recent case reports of IgG4-related HP, evidenced by IgG4-positive plasma cell infiltration, show a monophasic, steroid-responsive course.[20 21] Thus, ANCA-related and IgG4/MFS-related systemic diseases might be overlooked causes of HP.

Idiopathic HP showed a slight male predominance, while ANCA-related HP showed a female preponderance and IgG4/MFS-related HP had a marked male predominance, although there is no male or female preponderance in either ANCA-related[22 23] or IgG4/MFS-related systemic diseases.[24] ANCA-related HP cases had a higher age of onset than idiopathic HP cases and IgG4/MFS-related HP cases, probably reflecting the fact that age at onset of classical CSS patients among the Japanese is around 60 years, according to the results of a nationwide survey we previously conducted.[25] In terms of symptoms during the entire course, ANCA–related HP cases showed higher frequencies of fever and otological symptoms as initial symptoms, but lower frequencies of diplopia compared with idiopathic HP and IgG4/MFS-related HP cases. IgG4/MFS-related HP cases showed a higher frequency of cranial nerve involvement but less frequent sensory disturbance/decreased sensation. By contrast, idiopathic HP cases showed a higher frequency of double vision as an initial symptom and sensory disturbance/decreased sensation during the course. Thus, besides the differences in sex and age at onset, clinical manifestations are somewhat distinct among the three major groups of HP, which may be partly derived from the nature of the underlying diseases.

We conclude that ANCA-related disease and IgG4/MFS-related disease are the two major causes of HP in Japan. It is necessary to elucidate whether these findings, including an extremely high frequency of ANCA-related HP, are applicable to other races, by conducting large-scale epidemiological surveys in the future.

Contributors TY, HM and J-iK conceived the study, supervised the analyses and wrote the paper. TY and KS performed the statistical analyses. SU, TM, KM, NI, RY, MY, SK and KF participated in procedure development and collated the data.

Funding This study was supported in part by a Health and Labour Sciences Research Grant on Intractable Diseases (H23-Nanchitou (Nan)-Ippan-086) from the Ministry of Health, Labour and Welfare, Japan.

Competing interests TM has received speaker honoraria from Bayer Schering Pharma, Biogen Idec and Pfizer, and receives research support from Bayer Schering Pharma, the Ministry of Health, Labour and Welfare of Japan, the Japan Science and Technology Agency, the Ministry of Education, Science, Sports and Culture of Japan, and the Kaibara Morikazu Medical Science Promotion Foundation, Japan. SK has received honoraria from Teijin Pharma Limited, Nihon Pharmaceuticals Co Ltd, and Benesis Corporation. He is funded by research grants from the Ministry of Health, Labour and Welfare, Japan, and grants from the Ministry of Education, Culture, Sports, Science and Technology, Japan. J-iK is a consultant for Biogen Idec Japan, and has received honoraria from Bayer Healthcare and funding for a trip from Bayer Healthcare and Biogen Idec Japan. He is funded by a research grant for Nervous and Mental Disorders from the Ministry of Health, Labour and Welfare, Japan, and grants from the Japan Science and Technology Agency and the Ministry of Education, Culture, Sports, Science and Technology, Japan.

Ethics approval The study was approved by the Kyushu University Hospital ethical standards committee.

Provenance and peer review Not commissioned; externally peer reviewed.

REFERENCES

1 Kupersmith MJ, Martin V, Heller G, *et al*. Idiopathic hypertrophic pachymeningitis. *Neurology* 2004;62:686–94.
2 Dorr J, Elitok S, Dieste FJ, *et al*. Treatment-resistant chronic headaches and focal pachymeningitis in a 46-year-old man: a rare presentation of Wegener's granulomatosis. *Lancet Neurol* 2008;7:368–72.
3 Osoegawa M, Kira J, Fukazawa T, *et al*. Temporal changes and geographical differences in multiple sclerosis phenotypes in Japanese: nationwide survey results over 30 years. *Mult Scler* 2009;1:159–73.
4 Umehara H, Okazaki K, Masaki Y, *et al*. Comprehensive diagnostic criteria for IgG4-related disease (IgG4-RD), 2011. *Mod Rheumatol* 2012;22:21–30.
5 Hashimoto S, Fukutomi K, Nagai M, *et al*. Response bias in the nationwide epidemiological survey of an intracta- ble disease in Japan. *J Epidemiol* 1991;1:27–30.
6 Shobha N, Mahadevan A, Taly AB, *et al*. Hypertrophic cranial pachymeningitis in countries endemic for tuberculosis: diagnostic and therapeutic dilemmas. *J Clin Neurosci* 2008;15:418–27.
7 Murai H, Yamashita N, Watanabe M, *et al*. Characteristics of myasthenia gravis according to onset-age: Japanese nationwide survey. *J Neurol Sci* 2011;305:97–102.
8 Nozaki I, Hamaguchi T, Sanjo N, *et al*. Prospective 10-year surveillance of human prion diseases in Japan. *Brain* 2010;133:3043–57.
9 Iguchi A, Wada Y, Kobayashi D, *et al*. A case of MPO- and PR3-ANCA-positive hypertrophic cranial pachymeningitis with elevated serum IgG4. *Mod Rheumatol* 2013;23:151–5.